



Multifaceted characteristics of dryland aridity changes in a warming world

Xu Lian¹, Shilong Piao^{1,2,3}✉, Anping Chen^{4,5,6}, Chris Huntingford⁷, Bojie Fu^{8,9}, Laurent Z. X. Li¹⁰, Jianping Huang¹¹, Justin Sheffield¹², Alexis M. Berg¹³, Trevor F. Keenan^{14,15}, Tim R. McVicar^{16,17}, Yoshihide Wada¹⁸, Xuhui Wang¹, Tao Wang², Yuting Yang¹⁹ and Michael L. Roderick^{17,20}

Abstract | Drylands are an essential component of the Earth system and are among the most vulnerable to climate change. In this Review, we synthesize observational and modelling evidence to demonstrate emerging differences in dryland aridity dependent on the specific metric considered. Although warming heightens vapour pressure deficit and, thus, atmospheric demand for water in both the observations and the projections, these changes do not wholly propagate to exacerbate soil moisture and runoff deficits. Moreover, counter-intuitively, many arid ecosystems have exhibited significant greening and enhanced vegetation productivity since the 1980s. Such divergence between atmospheric and ecohydrological aridity changes can primarily be related to moisture limitations by dry soils and plant physiological regulations of evapotranspiration under elevated CO₂. The latter process ameliorates water stress on plant growth and decelerates warming-enhanced water losses from soils, while simultaneously warming and drying the near-surface air. We place these climate-induced aridity changes in the context of exacerbated water scarcity driven by rapidly increasing anthropogenic needs for freshwater to support population growth and economic development. Under future warming, dryland ecosystems might respond non-linearly, caused by, for example, complex ecosystem–hydrology–human interactions and increased mortality risks from drought and heat stress, which is a foremost priority for future research.

Drylands describe regions subject to permanent or seasonal water deficiency, which currently occupy ~42% of global land surface^{1–4}. They are typically located in subtropical regions characterized by air mass divergence, in the rain shadow of mountain chains or in the middle of continental land masses⁵ (FIG. 1). Dryland ecosystems have a critical role in the global carbon cycle, dominating the trend and variability of global terrestrial carbon sink, owing to their high sensitivity to inter-annual climate variability⁶. Moreover, they are home to ~30% of the world's endangered and endemic species^{7,8}, and are, thus, critical to global biodiversity conservation efforts. Drylands also provide staple food, cotton, timbers and livestock to support nearly 2.5 billion people^{1,3,8}, among whom about half live below the United Nations poverty line.

The sustainability of ecosystem services and societal goods provided by global drylands, however, is threatened by ongoing anthropogenic warming^{1,2,9}. Indeed, the limited socio-economic capacity for adaptation and mitigation^{9,10}, together with the faster-than-average

warming rate^{2,11,12}, makes drylands among the most vulnerable regions to climate change. As such, concerns about the fate of dryland socio-ecological systems have been a priority for important global initiatives, including the Global Dryland Ecosystem Programme¹³, the Intergovernmental Science-Policy Platform on Biodiversity and Ecosystem Services¹⁴, the United Nations Convention on Biological Diversity¹⁵, the United Nations Sustainable Development Goals¹⁶ and the Intergovernmental Panel on Climate Change³.

A surge of research has, therefore, emerged to assess dryland changes in the past and predict their future trajectories, the findings of which are highly contradictory. For example, numerous studies suggest that global drylands have become more arid^{10,17–26}, yet, others show the same regions experiencing greening and enhanced vegetation activity^{6,27–33}. This apparent inconsistency stems from different interpretations of aridity — the state of insufficient water supply to meet demand^{34,35} — dependent on whether it is used in an atmospheric, agricultural, hydrologic or ecological context (BOX 1).

Q1
Q2
Q3
Q4

✉e-mail: slpiao@pku.edu.cn
<https://doi.org/10.1038/s43017-021-00144-0>

Key points

- Atmospheric, agricultural, hydrological and ecological indices of aridity reveal strongly divergent trends since 1950 and into the near future.
- Warming-driven increases in vapour pressure deficit hasten evaporative water loss and deplete surface moisture, in turn, amplifying atmospheric drying through land–atmosphere feedbacks.
- Plant stomatal closure under elevated CO₂ reduces transpiration and compensates for the adverse effect of higher vapour pressure deficit for plant growth, explaining the co-occurrence of ecosystem greening and atmospheric drying in drylands.
- The physiologically induced lowering of evapotranspiration under rising CO₂, along with the strong limitation by soil moisture, disconnects atmospheric drying and hydrological responses in drylands.
- With rapid climate change and population growth, anthropogenic water demand in drylands is projected to increase by ~270% by the 2090s, exacerbating current water resource scarcity.
- As future water deficits are driven mainly by increasing water demand, sustainable water resource management and water conservation technologies are needed to balance the socio-economic demands for water resources, while maintaining healthy dryland ecosystems.

The associated demand and supply sides of aridity, as well as the physical and/or biological processes driving changes of both sides, vary considerably among these different interpretations.

In this Review, we reconcile disagreements between aridity metrics by acknowledging the multifaceted nature of water supply and demand for the atmosphere, hydrological systems, ecosystems and human society over global drylands, as well as their interconnections^{35–37},

knowledge of which will allow for more effective adaptation policies. We first provide an overview of how aridity and the extent of global drylands have changed since the 1950s and are projected to change in the future, presenting contrasting findings according to atmospheric, agricultural, hydrological or ecological dryland definitions. We next discuss the attribution of aridity changes to physical and physiological processes within the dryland system, arguing that strong soil moisture limitations, together with ecosystem physiological regulations of hydrological cycles under rising atmospheric CO₂, can explain the apparent conflicting viewpoints. We then outline the central role of humans in water resource utilization and evaluate dryland management policy decisions under the intensification of ecosystem–hydrology–human interactions. We end with a forward-looking perspective on future dryland research.

Historical aridity changes in drylands

The growth of global data from remote sensing and in situ networks, along with sophisticated climate–carbon cycle modelling, provides valuable new datasets and tools for assessing long-term surface aridity changes^{38,39} (Supplementary Table 1). A large body of research uses the aridity index, AI^{10,17,21,22,24,40–43}, which represents the balance between water received by the land surface (precipitation) and that demanded by the atmosphere (potential evapotranspiration, PET) (BOX 1). However, it has been suggested that the AI could be problematic in depicting surface aridity changes, being too simplistic to capture the full complexity of aridity^{40,44,45}.

Hence, there is an increasing recognition that aridity should be evaluated using a more diverse representation of water demand and supply for different land surface processes^{36,40,46}. Four alternative aridity metrics have, thus, been increasingly employed, including: vapour pressure deficit (VPD), which measures the atmospheric water demand; soil moisture, which describes the soil water supply to support ecosystem function and agricultural production; runoff, which signifies the volume of freshwater available for drinking, irrigation, industry and other societal needs; and vegetation productivity and/or greenness, a robust indicator of ecological aridity, given the primary role of water in determining dryland vegetation productivity²⁸.

With these five aridity metrics, as quantified by observations and state-of-the-art model simulations (12 offline dynamic global vegetation models, DGVMs, and 23 Earth system models, ESMs, from the Coupled Model Intercomparison Project Phase 5, CMIP5; Supplementary Tables 2,3), two approaches are used to assess dryland aridity changes since the 1950s and projections into the future (FIG. 2). The first takes zonal average values of different aridity metrics over global drylands, while assuming a fixed global dryland extent (as in FIG. 1). The second calculates the evolving fraction of global water-stressed area, applying a fixed threshold to each aridity metric to derive a temporally variable dryland extent (Supplementary Methods; Supplementary Figs 1–3). In the second approach, the fraction of global water-stressed area is denoted as f_{atm} , f_{AI} , f_{soil} , f_{hyd} and f_{veg} , for aridity metrics defined by VPD, AI, soil moisture,

Author addresses

¹Sino-French Institute for Earth System Science, College of Urban and Environmental Sciences, Peking University, Beijing, China.

²Key Laboratory of Alpine Ecology, Institute of Tibetan Plateau Research, Chinese Academy of Sciences, Beijing, China.

³Center for Excellence in Tibetan Plateau Earth Sciences, Chinese Academy of Sciences, Beijing, China.

⁴Department of Biology, Colorado State University, Fort Collins, CO, USA.

⁵Graduate Degree Program in Ecology, Colorado State University, Fort Collins, CO, USA.

⁶Woodwell Climate Research Center, Falmouth, MA, USA.

⁷UK Centre for Ecology & Hydrology, Wallingford, UK.

⁸State Key Laboratory of Urban and Regional Ecology, Research Center for Eco-Environmental Sciences, Chinese Academy of Sciences, Beijing, China.

⁹State Key Laboratory of Earth Surface Processes and Resource Ecology, Faculty of Geographical Science, Beijing Normal University, Beijing, China.

¹⁰Laboratoire de Météorologie Dynamique, CNRS, Sorbonne Université, Ecole Normale Supérieure, Ecole Polytechnique, Paris, France.

¹¹Key Laboratory for Semi-Arid Climate Change of the Ministry of Education, College of Atmospheric Sciences, Lanzhou University, Lanzhou, China.

¹²Department of Geography, University of Southampton, Southampton, UK.

¹³Department of Earth and Planetary Sciences, Harvard University, Cambridge, MA, USA.

¹⁴Earth and Environmental Sciences Area, Lawrence Berkeley National Laboratory, Berkeley, CA, USA.

¹⁵Department of Environmental Science, Policy, and Management, University of California, Berkeley, Berkeley, CA, USA.

¹⁶CSIRO Land and Water, Canberra, ACT, Australia.

¹⁷Australian Research Council Centre of Excellence for Climate Extremes, Canberra, ACT, Australia.

¹⁸International Institute for Applied Systems Analysis, Laxenburg, Austria.

¹⁹State Key Laboratory of Hydrosience and Engineering, Department of Hydraulic Engineering, Tsinghua University, Beijing, China.

²⁰Research School of Earth Sciences, Australian National University, Canberra, ACT, Australia.

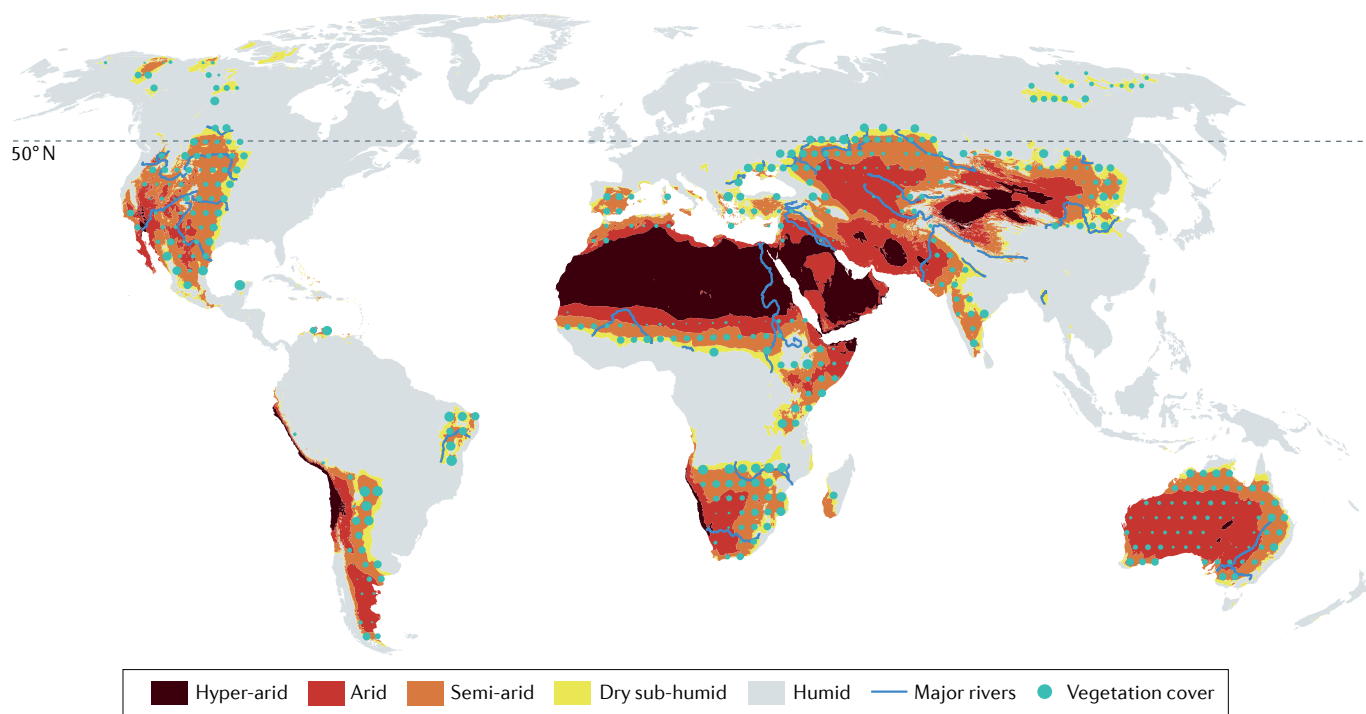


Fig. 1 | **Global drylands and ecohydrological conditions.** The extent and classification of aridity-index-defined drylands for 1961–1990, based on the TerraClimate dataset with high (~4-km) spatial resolution¹⁷². The cyan dots illustrate the density of vegetation cover for 1982–1990 (based on the GIMMS normalized difference vegetation index), with larger dots indicating denser vegetation cover. Note that all analyses in FIGS 2,3 focus solely on warm drylands (drylands south of 50°N), where all land surface elements routinely experience water stress.

runoff and vegetation productivity, respectively. Aridity changes of global drylands using these different metrics are now quantified and compared.

Ubiquitous atmospheric drying. VPD is defined as the difference between saturated water vapour pressure (which increases exponentially with air temperature) and actual water vapour pressure (which is a function of air humidity). Hence, VPD measures how far the air is from thermodynamic equilibrium, with high values related to strong atmospheric demand for water from land and/or water surfaces. Research into VPD changes consistently indicates an increasing trend of global dryland atmospheric aridity^{47–49}, as confirmed by various observational datasets (Supplementary Figure 4). On average, global dryland VPD shows a statistically significant increase of 0.012 ± 0.001 kPa per decade ($p < 0.05$) over 1948–2016 (FIG. 2a; TABLE 1), as also reproduced by ESMs (0.015 ± 0.002 kPa per decade, $p < 0.05$). Consistent with the overall VPD increase, the global dryland area exposed to atmospheric water stress, as defined by VPD-based f_{atm} , similarly exhibits an increasing trend of $0.55 \pm 0.11\%$ per decade ($p < 0.01$) over the same time period (FIG. 2f; TABLE 1). As dryland surfaces warm 20–40% faster than humid regions⁴¹, the increase in VPD is amongst the highest values on the global land surface, ~25% higher than humid regions^{48,49}.

Land surface drying characterized by the standard aridity index. Traditionally, the most widely used metric to examine surface aridity was the AI^{10,21,24,42}, whereby a

lower value corresponds to higher aridity, and is often interpreted as a higher risk of desertification and land degradation^{3,10,50–52}. Observational and modelling-based AI studies generally point to an enhanced drying trend since the pre-industrial era, signifying an expansion of dryland area (as defined by a standard threshold of $\text{AI} \leq 0.65$)^{10,22,24} (Supplementary Table 1). For example, gauge-based precipitation and reanalysis-based PET data suggest a 2.4×10^6 km² expansion of global drylands when comparing 1991–2005 to the 1950s (REF²⁴), the strongest regional increases of which occurred in southern Africa, the Sahel and North China^{10,24}. This surface drying trend is confirmed through analyses using multiple combinations of precipitation and PET datasets (FIG. 2b), translating into an ensemble mean global expansion of dryland area (f_{AI}) by $0.13 \pm 0.06\%$ per decade ($p < 0.05$) over 1948–2016 (FIG. 2g; TABLE 1). However, the reported dryland aridity increase and dryland expansion are highly sensitive to selected inputs of observational data products^{38,53}. For instance, the magnitude of the estimated expansion rate has a large spread across different data streams, ranging from near zero to 0.60% per decade (TABLE 1). The previously reported rate of 0.57% per decade (REFS^{10,24}) falls into this range but is close to the upper boundary.

While multi-data combinations provide a complete assessment of possible AI changes, they cannot ensure the physical consistency between precipitation and other meteorological variables involved in PET calculation⁵³. Assessments with climatic diagnostics from ESMs generally do not have this physical inconsistency. Indeed,

Box 1 | The multifaceted features and definitions of 'aridity'

Aridity is a long-term state of water scarcity, which measures “the degree to which a climate lacks effective, life-promoting moisture”¹⁷⁵. In this sense, aridity is essentially different from drought, which tracks short-term (days to years) departures from normal surface water conditions. Owing to the limited availability of surface soil moisture measurements, the aridity index (AI), which only requires meteorological measurements, is popular in dryland studies. The AI calculates the balance between the atmospheric water supply to the land (precipitation) and its demand from the land surface (potential evapotranspiration, PET). The PET formulation is often based on the Penman–Monteith equation¹⁷⁶, which requires meteorological inputs of net solar radiation (R_n), temperature (T), vapour pressure deficit (D), 2-m wind speed (u_2), psychrometric constant (γ) and the slope of saturation vapour pressure with temperature (Δ) (Eq. 1):

$$PET = \frac{0.408\Delta R_n + \gamma \frac{900}{T+273} u_2 D}{\Delta + \gamma \left(1 + (0.34 + 0.00024(c_a - 300))u_2\right)} \quad (1)$$

where $0.00024(c_a - 300)$ accounts for the effect of rising atmospheric CO₂ concentration (c_a , ppm) on surface stomatal resistance (fixed as 0.34 in the original PET parameterization), with the coefficients estimated from CMIP5 model outputs forced by rising c_a under non-water-stressed conditions⁴⁵. Drylands are traditionally defined by the United Nations Environment Programme⁴⁷ as areas with $AI \leq 0.65$, and can be further subcategorized into dry sub-humid ($0.65 > AI \geq 0.5$), semi-arid ($0.5 > AI \geq 0.2$), arid ($0.2 > AI \geq 0.05$) and hyper-arid ($AI < 0.05$) regions^{10,42}.

Importantly, aridity itself is a highly complex concept on which there are numerous specific perspectives. Atmospheric aridity describes high atmospheric demand for water, and is measured by vapour pressure deficit or relative humidity^{48,72}; soil moisture (or agricultural) aridity describes a state of soil moisture stress^{57,177}; hydrological aridity describes a deficit of surface runoff⁷⁸; ecological aridity describes a state of insufficient moisture to support vegetation growth, and is often related to reduction (or reduced capacity) of plant photosynthetic uptake of CO₂ (REF.³⁶).

Although aridity means an excess of water demand over available supply for all Earth system processes, both the demand and supply sides differ substantially among them^{36,37,40,46,155}. For instance, soil moisture is supplied by precipitation and glacier meltwater, and the water demand is determined by plant transpiration and soil evaporation. Plants extract moisture from soils to live and grow, and the water demand is determined by atmospheric dryness and plant physiology³⁷. Livestock and humans demand water to survive, which is provided mostly by rivers, lakes and groundwater reservoirs. Such different Earth system processes involved in the depiction of demand and supply for water cause these metrics to diverge in response to elevated CO₂.

the observed AI decrease and associated expansion of dryland extent are broadly reproduced by ESMs^{10,24}. For example, CMIP5 ESMs estimate an expansion of $0.14 \pm 0.03\%$ per decade ($p < 0.05$) during 1948–2005 (FIG. 2g; TABLE 1), consistent with the ensemble mean of multiple empirical data combinations ($0.13 \pm 0.06\%$ per decade). For both observations and models, the expanding rate of global dryland extent based on the AI is much slower than that based on VPD for the same period (FIG. 2f,g).

In addition, the AI is commonly calculated using the Penman–Monteith equation (BOX 1), now thought to overestimate PET changes under elevated CO₂ because it incorrectly assumes a fixed resistance for vegetated surfaces^{40,45,54,55}. The introduction of a CO₂-responsive surface resistance to the Penman–Monteith-based PET parameterization lowers PET increases (though it is still larger than concurrent precipitation increases⁴⁰), and the resultant AI shows higher consistency with modelled hydrological changes⁴⁵. Accounting for the CO₂ effect in the PET formulation thus leads to a ~40% reduction in the estimated increase in AI-based dryland extent during 1948–2016. As such, the resulting long-term trend becomes statistically insignificant at

$0.08 \pm 0.06\%$ per decade (FIG. 2g; TABLE 1). However, caution is needed when utilizing the modified PET model in dryland assessments, as the model-based estimate of CO₂ effect on surface resistance has not been experimentally validated⁴⁵. With this limitation in mind, it is anticipated that the CO₂-modified PET model underestimates dryland PET increase and, thus, the rate of dryland expansion. Therefore, the rate of AI-based dryland expansion should fall between the estimates with and without accounting for the CO₂ impacts on PET, that is, between 0.08 and 0.13% per decade.

Relatively weak total-column soil moisture drying. Soil moisture levels determine water stress for natural and agricultural ecosystems. Remote sensing by microwave and gravimetric sensors, and its application in numerical land data assimilation schemes, now offers a useful way to monitor soil moisture dynamics at large spatial scales. However, there remain limitations with current technology, including limited vertical sampling depth and low accuracy over densely vegetated surfaces for microwave-based retrievals^{56,57}. Hence, compared with the more robust finding of aridification and dryland expansion based on VPD or the AI, aridity changes based on soil moisture often show divergent signs, depending on the data used, the period investigated and the soil depth involved.

Using microwave satellite observations of near-surface soil moisture, it is estimated that 38.4% of global drylands have experienced a significant drying trend since 1979, while only 2.9% showed a wetting trend⁵⁸. However, other observation-driven datasets of total-column (or root-zone) soil moisture (such as GLEAM, TerraClimate and GLDAS, see Supplementary Methods) consistently reveal an increasing trend for the same period

Fig. 2 | Past and future dryland changes evaluated by five different aridity metrics. a–e | Various observational and model-derived anomalies of vapour pressure deficit (VPD) (panel a), aridity index (AI) or AI_CO₂ that additionally accounts for CO₂ physiological impacts (panel b), soil moisture (panel c), runoff (panel d) and gross primary production (GPP), normalized difference vegetation index (NDVI) and leaf area index (LAI) (panel e), all averaged over AI-defined baseline regions of drylands for 1961–1990. **f–j** | As in panels a–e, but anomalies of the fraction of water-stressed land areas (drylands) evaluated by VPD (f_{atm}) (panel f), AI (f_{AI} or $f_{AI_CO_2}$) (panel g), soil moisture (f_{soil}) (panel h), runoff (f_{hyd}) (panel i) and GPP, NDVI or LAI (f_{veg}) (panel j). Similar to f_{AI} (regions with $AI < 0.65$), f_{atm} , f_{soil} , f_{hyd} and f_{veg} are computed using threshold values of the corresponding metric (Supplementary Methods). Anomalies are computed by subtracting the climatological mean of 1961–1990 (or a subset of years during this period, depending on the temporal coverage of data). The shaded areas represent the 95% confidence intervals of multiple data sources (for VPD and AI) or model results (for dynamic global vegetation models (DGVMs) or Earth system models (ESMs)). The ESM results are derived from CMIP5 under the ‘historical’ (1948–2005) and ‘RCP4.5’ (2006–2100) scenarios. These different metrics present divergence in aridity changes and rates of global dryland expansion in both the past and the future. Trends of each metric and dataset are summarized in TABLE 1.

(FIG. 2c; TABLE 1). The divergence of soil moisture trends is likely because surface and deep-layer soil moistures are controlled by different processes — warming-induced rise in evaporative demand drives the reduction of surface soil moisture, whereas soil moisture in deep layers is more controlled by antecedent moisture status and vegetation activities^{59–61}. Weaker drying in the root zone compared with the surface soil suggests that deep-rooted plants in

drylands are less likely to suffer severe soil moisture stress than shallow-rooted plants and crops.

Over 2002–2016, gravimetric sensors onboard NASA’s Gravity Recovery and Climate Experiment satellites, however, detect a robust decline of endorheic water storage²⁰ by about 106.3 Gt per year, most of which is in drylands. Central Eurasia contributes most (69%) to this decline, followed by the Sahara desert, the Dry Andes,

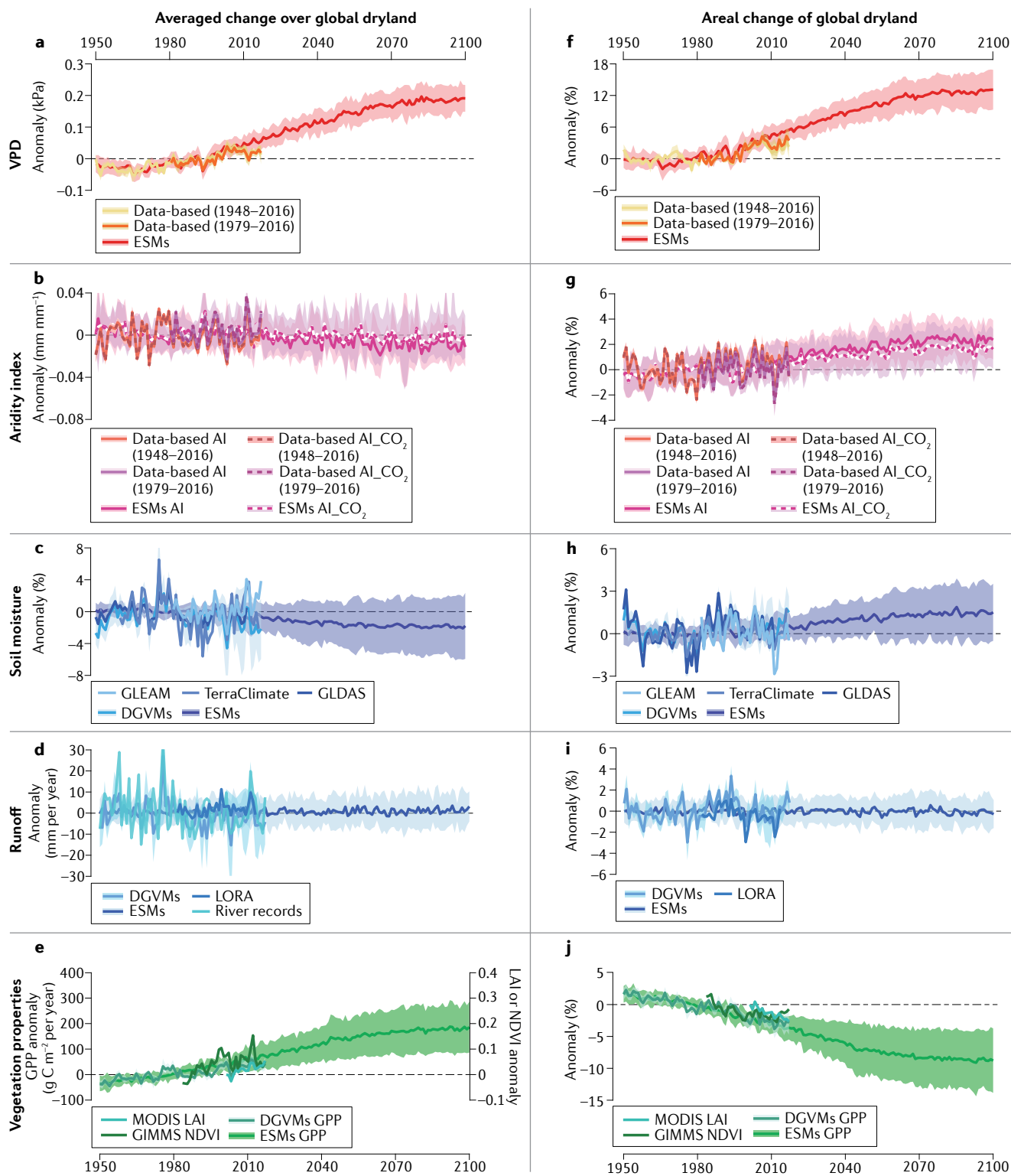


Table 1 | Trend statistics for different aridity metrics and databases

Metric and database	Averaged change over the global dryland			Areal change of the global dryland (% per decade)		
	1948–2016	1979–2016	Near future	1948–2016	1979–2016	Near future
Data-based VPD (10 ⁻² kPa per year)	0.12 ± 0.01 (**)	0.16 ± 0.02 (**)	–	0.55 ± 0.11 (**)	1.49 ± 0.19 (**)	–
ESMs VPD (10 ⁻² kPa per year)	0.15 ± 0.002 (1948–2005, **)	0.25 ± 0.04 (1979–2005, **)	0.21 ± 0.01 (2006–2100, **)	0.65 ± 0.07 (1948–2005, **)	1.15 ± 0.21 (1979–2005, **)	1.01 ± 0.03 (2006–2100, **)
Data-based AI (10 ⁻³ per year)	–0.02 ± 0.08 (n.s.)	–0.13 ± 0.12 (n.s.)	–	0.13 ± 0.06 (**)	0.05 ± 0.15 (n.s.)	–
Data-based AI_CO ₂ (10 ⁻³ per year)	0.04 ± 0.08 (n.s.)	0.20 ± 0.12 (n.s.)	–	0.08 ± 0.06 (n.s.)	–0.02 ± 0.15 (n.s.)	–
ESMs AI (10 ⁻³ per year)	–0.07 ± 0.04 (1948–2005, *)	0.16 ± 0.15 (1979–2005, n.s.)	–0.11 ± 0.02 (2006–2100, **)	0.14 ± 0.03 (1948–2005, **)	0.02 ± 0.10 (1979–2005, *)	0.20 ± 0.02 (2006–2100, **)
ESMs AI_CO ₂ (10 ⁻³ per year)	–0.03 ± 0.04 (1948–2005, n.s.)	0.20 ± 0.15 (1979–2005, n.s.)	–0.07 ± 0.02 (2006–2100, **)	0.11 ± 0.03 (1948–2005, **)	–0.03 ± 0.10 (1979–2005, n.s.)	0.15 ± 0.01 (2006–2100, **)
GLDAS soil moisture (% per year)	–0.015 ± 0.007 (1948–2010, **)	0.014 ± 0.016 (1979–2010, n.s.)	–	0.09 ± 0.08 (1948–2010, n.s.)	–0.12 ± 0.18 (1979–2010, n.s.)	–
TerraClimate soil moisture (% per year)	–0.061 ± 0.038 (1980–2016, n.s.)	0.032 ± 0.052 (1980–2016, n.s.)	–	0.05 ± 0.05 (1958–2015, n.s.)	–0.12 ± 0.10 (1979–2015, n.s.)	–
GLEAM soil moisture (% per year)	–	0.047 ± 0.022 (1980–2016, **)	–	–	–0.22 ± 0.16 (1980–2016, n.s.)	–
DGVMs soil moisture (% per year)	–0.017 ± 0.009 (**)	–0.045 ± 0.017 (n.s.)	–	0.09 ± 0.05 (*)	0.13 ± 0.10 (n.s.)	–
ESMs soil moisture (% per year)	–0.010 ± 0.002 (1948–2005, **)	–0.026 ± 0.006 (1979–2005, **)	–0.014 ± 0.001 (2006–2100, **)	0.05 ± 0.02 (1948–2005, **)	0.06 ± 0.05 (1979–2005, n.s.)	0.13 ± 0.01 (2006–2100, **)
River records (mm year ⁻²)	–0.192 ± 0.120 (1948–2016, n.s.)	0.203 ± 0.190 (1948–2016, n.s.)	–	–	–	–
LORA runoff (mm year ⁻²)	–	0.106 ± 0.055 (1980–2012, *)	–	–	–0.33 ± 0.16 (1980–2012, **)	–
DGVMs runoff (mm year ⁻²)	–0.075 ± 0.038 (**)	0.012 ± 0.076 (n.s.)	–	0.06 ± 0.07 (n.s.)	–0.21 ± 0.16 (n.s.)	–
ESMs runoff (mm year ⁻²)	–0.005 ± 0.010 (1948–2005, n.s.)	0.021 ± 0.036 (1979–2005, n.s.)	0.011 ± 0.005 (2006–2100, **)	0.03 ± 0.02 (1948–2005, *)	–0.17 ± 0.08 (1979–2005, **)	–0.02 ± 0.01 (2006–2100, *)
GIMMS NDVI (10 ⁻² per year)	–	0.024 ± 0.006 (1982–2016, **)	–	–	–0.64 ± 0.14 (1982–2016, **)	–
MODIS LAI (10 ⁻² per year)	–	0.33 ± 0.06 (2000–2016, **)	–	–	–1.55 ± 0.19 (2000–2016, **)	–
DGVMs GPP (g C m ⁻² year ⁻²)	1.0 ± 0.1 (**)	1.4 ± 0.2 (**)	–	–0.72 ± 0.04 (**)	–0.95 ± 0.10 (**)	–
ESMs GPP (g C m ⁻² year ⁻²)	1.5 ± 0.0 (1948–2005, **)	1.6 ± 0.1 (1979–2005, **)	1.4 ± 0.0 (2006–2100, **)	–0.75 ± 0.02 (1948–2005, **)	–0.95 ± 0.06 (1979–2005, **)	–0.67 ± 0.02 (2006–2100, **)

Slope (±1 standard deviation) and statistical significance of the linear regression against time for each aridity metric and database. Unless otherwise stated in parentheses, the period over which trends are quantified are shown in the column heading. Statistical significance is determined using a *t*-test, with symbols ‘***’, ‘**’ and ‘n.s.’ denoting *p* < 0.05, *p* < 0.1 and *p* > 0.1, respectively. Trends for vapour pressure deficit (VPD) and aridity index (AI) are calculated using the mean of multiple datasets, and those for dynamic global vegetation models (DGVMs) and Coupled Model Intercomparison Project Phase 5 (CMIP5) Earth system models (ESMs) using the mean of multiple models. Note that the trend unit for averaged change is metric-dependent, but that, for areal change, it is the same across metrics (% per decade). GPP, gross primary production; LAI, leaf area index; NDVI, normalized difference vegetation index.

Australia and western USA, while water gains were found in the Great Rift Valley and southern Africa²⁰. This signal of endorheic water loss reflects an overall reduction of soil moisture, surface water and groundwater levels, likely attributable to decadal or longer climate variability and human influence^{20,62}.

Despite strong model dependencies, soil moisture estimated by climate models also generally show a decreasing trend over drylands^{59,63,64}. The model-derived trend is qualitatively similar in pattern to the AI⁶³ and extends for both surface soils and the total soil column, although being more significant for the former^{59,60}. As such, the global land area under (total-column) soil moisture stress predicted by both DGVMs and CMIP5 ESMs is increasing at 0.09 ± 0.05% per decade (*p* = 0.05)

and 0.05 ± 0.02% per decade (*p* < 0.05), respectively, over 1948–2016 (FIG. 2h; TABLE 1). The rate of dryland expansion inferred from modelled total soil moisture is substantially smaller than that from VPD or the AI. Hence, the increased atmospheric evaporative demand has not fully translated to increased soil moisture deficits across all soil layers, despite its dominance on the enhanced soil moisture deficits at the near-surface layer^{59,60}.

Regionally divergent runoff changes. Along with deep groundwater resources, surface runoff is an important source of freshwater for societal demands of agricultural and industrial production in drylands. Unlike the ubiquitous increase in surface aridity inferred from the VPD and AI metrics, runoff generally reveals divergent

regional changes^{44,65,66}, suggesting spatially heterogeneous hydroclimatic drivers and runoff responses.

Surface runoff of most dryland rivers is decreasing^{19,65,67–69}. Indeed, through aggregating streamflow records of the world's largest rivers flowing through drylands (Supplementary Table 4), an overall declining trend in streamflow of -0.19 ± 0.12 mm per year ($p=0.11$, or -11.9%) is apparent during 1948–2016 (FIG. 2d; TABLE 1). In general, regions experiencing rapid runoff decreases often overlap with those under intense human influences, such as the Yellow River in North China⁶⁷, the Guadalquivir River in Spain, the Murray River in south-eastern Australia and the Indus River in Pakistan⁷⁰ (Supplementary Table 4). Simulations by both DGVMs and CMIP5 ESMs agree with the observed overall decline (FIG. 2d; TABLE 1). Consequently, there is an increase of modelled land area subject to hydrological aridity evaluated by runoff deficits (f_{hyd}), reaching $0.06 \pm 0.07\%$ per decade ($p>0.10$) for DGVMs and $0.03 \pm 0.02\%$ per decade ($p<0.10$) for ESMs (FIG. 2i; TABLE 1). Achieving a high statistical significance is, however, precluded by the strong decadal climate variability and spatial heterogeneity.

Nevertheless, increases in runoff have also been observed for about 20% of large rivers in arid regions⁶⁵, such as the Daly River in north Australia and the Tana River in Kenya⁷⁰. This runoff increase has been even more widespread since the 1980s, driven by concurrent precipitation increases, as supported by both observational streamflow records⁷⁰ and a gridded synthesis runoff product⁷¹ (FIG. 2i; TABLE 1).

Reduced water stress for dryland vegetation. Increased VPD indicates a higher vapour pressure gradient between leaves and the atmosphere, enhancing water loss by plant transpiration^{49,72}. However, plants can also modify their water need through physiological adjustments over both shorter and longer timescales, for example, through regulating stomatal conductance and changing leaf area, respectively^{19,32,37}. In drylands, how well plants adapt to changing hydrological regimes and, consequently, how well they grow depends on whether the altered water supply is sufficient to meet their demand, which, itself, could be evolving³⁷. Considering that water stress, owing to the insufficient water supply to meet the demand, is the primary factor limiting dryland vegetation growth, the outcome of vegetation changes provides a useful surrogate metric for evaluating ongoing water stress of dryland vegetation.

Vegetation greenness indices from satellite observations (for example, the leaf area index, LAI, and the normalized difference vegetation index, NDVI) consistently show a significant positive trend in dryland foliage cover since the 1980s^{28–30}, co-occurring with the enhanced atmospheric aridity indicated by VPD and the AI. This enhanced dryland vegetation growth has remained strong into the twenty-first century, as confirmed by greenness indices from the well-calibrated MODIS Collection 6 (FIG. 2e) and SPOT satellite data^{32,73}. Some regional hotspots of vegetation greening also overlap with drylands under intensive agricultural expansion, such as in India, the North China Plain, the US Great Plains and south-east Australia^{32,73}.

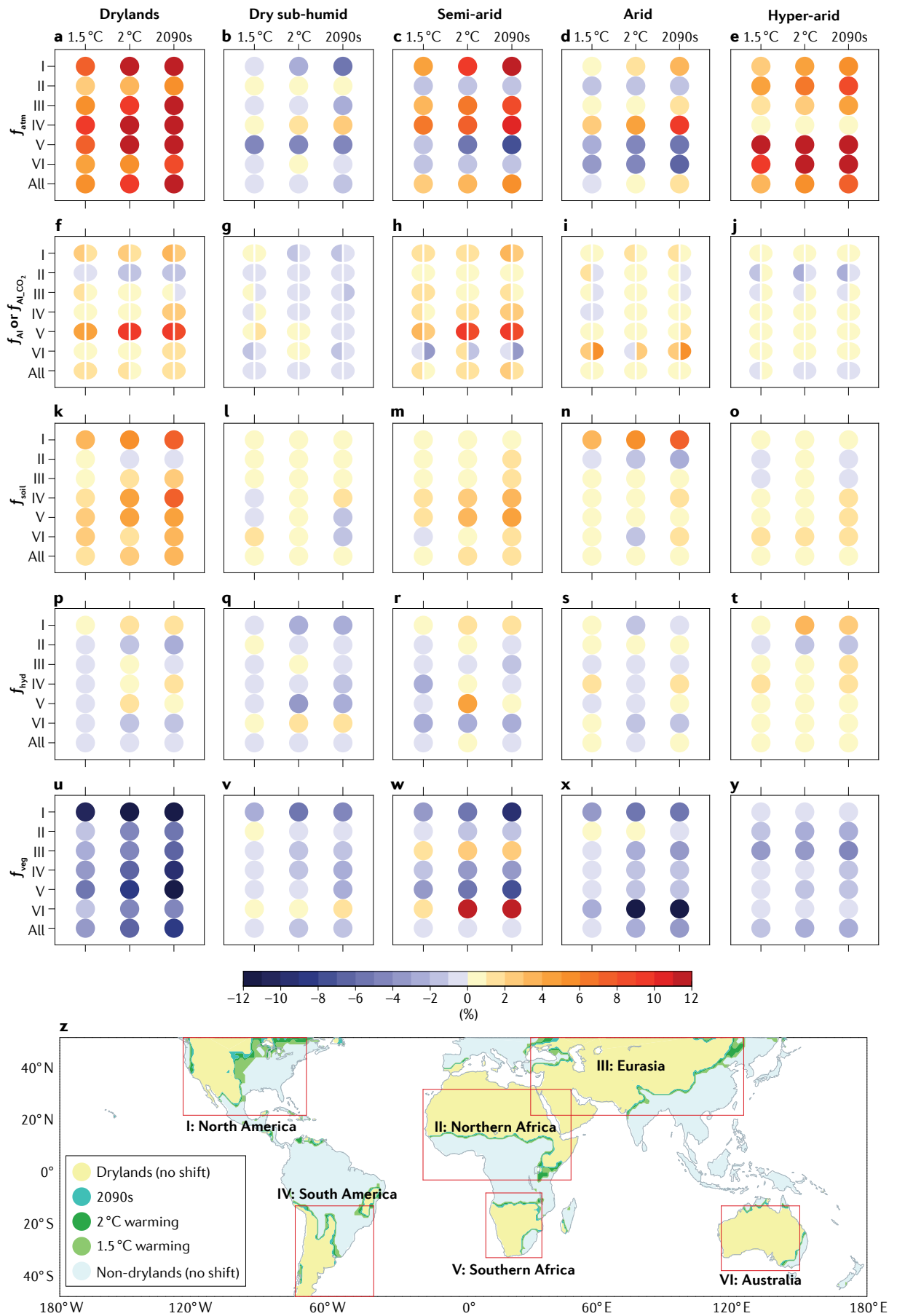
Furthermore, above-ground production of dryland ecosystems, based on both empirical observation-based product and process-based models, also presents an increasing trend that accounts for over 50% of the increase in global carbon sink during 1982–2011 (REF.⁶) (FIG. 2e; TABLE 1). Dryland gross primary production simulated by DGVMs and ESMs also increases at a rate of 0.6 Pg C per decade and 1.0 Pg C per decade, respectively. Such changes correspond to an overall reduction in the areal coverage of vegetation-growth-defined drylands (f_{veg}) by 4.8% (for DGVMs) and 5.5% (for ESMs) over 1948–2005 (FIG. 2j; TABLE 1), in contrast to the areal increases implied by f_{VPD} and f_{AI} .

Thus, a holistic overview of changes in surface aridity and dryland extent suggests that aridity changes involve multidimensional land surface responses to climate change, which could not be captured by any single, offline aridity metric. This fact is particularly critical for dryland assessment, as different indices point to highly divergent aridity changes and rates of dryland expansion in recent decades. Specifically, dryland soil moisture and surface runoff decrease following near-surface atmospheric drying (based on VPD), albeit with substantial uncertainties and regional heterogeneity. In contrast, satellite records and models consistently illustrate a greening and more productive trend in the warmer and CO₂-enriched drylands.

Future aridity changes in drylands

With atmospheric and land surface drying observed since around the 1950s, there is clear interest in understanding how dryland aridity conditions will change with future warming. Indeed, given that water resource shortage is the major constraint to socio-economic growth and ecological security in drylands, understanding future aridity changes is critical to regionally targeted adaptation planning and decision-making^{17,41}. ESMs provide sufficient climate and land surface diagnostics to allow for systematic assessment of future aridity metrics, and have been widely tested and used^{10,17,24,40,63}. To better understand dryland projections under various temperature thresholds, we quantify the percentage change in dryland area for different aridity metrics (f_{atm} , f_{AI} , f_{soil} , f_{hyd} and f_{veg}) in different regions using CMIP5 ESM projections (FIG. 3).

CMIP5-projected changes. AI-based aridity projections with CMIP5 models estimate a persistent increase of global dryland extent by ~1–4%, depending on the temperature threshold used (FIGS 2g,3f). These changes are broadly consistent with previous analyses, which suggest a 4% and 10% increase of global dryland extent by 2100 relative to 1961–1990 under RCP4.5 (an intermediate emission scenario) and RCP8.5 (a high-end emission scenario), respectively²⁴. Indeed, when anthropogenic warming is over 1.5°C above pre-industrial, the signal of increased aridity can be distinguished from natural variability for 8% and 24% of the global land surface for the two scenarios; for 2°C warming, these values increase to 10% for RCP4.5 and 32% for RCP8.5 (REF.¹⁷). However, this expansion is not spatially uniform; for example, up to 10% increases in dryland extent are projected for



◀ **Fig. 3 | Continental assessment of future dryland changes.** Projected future changes in the fraction of drylands and the four dryland subcategories (dry sub-humid, semi-arid, arid and hyper-arid; columns), as presented by f_{atm} (panels **a–e**), f_{AI} and $f_{\text{AI,CO}_2}$ (panels **f–j**, left and right half of symbols, respectively), f_{soil} (panels **k–o**), f_{hyd} (panels **p–t**) and f_{veg} (panels **u–y**). Each circle represents the difference between dryland area (as a percentage of the subcontinent area) of a future period (1.5 °C or 2 °C warmer than the pre-industrial level, or the 2090s; all under the CMIP5 RCP4.5 scenario) and that of the 1961–1990 baseline (under the CMIP5 historical scenario). Changes in f_{atm} , f_{soil} , f_{hyd} and f_{veg} are computed using threshold values of the corresponding metric (Supplementary Methods). Continental dryland regions labelled I–VI are marked with red boxes in panel **z**, which also illustrates the spatial distribution of regions where vegetation growth indicates a conversion from drylands to non-drylands in the near future (for 1.5 °C warmer, 2 °C warmer or the 2090s, relative to 1961–1990), corresponding to panels **u–y**. It is projected that, in the future, the global dryland area will expand based on f_{atm} , f_{AI} and f_{soil} , but contract based on f_{hyd} and f_{veg} , with regionally dependent magnitude and/or sign of changes.

southern Africa with 2 °C warming, whereas a reduction of ~2% is anticipated for northern Africa (FIG. 3f).

Global drylands are commonly divided into four subcategories (hyper-arid, arid, semi-arid and dry sub-humid) based on a range of AI thresholds¹⁰ (BOX 1). Among these four subcategories, semi-arid and arid regions are estimated to expand in area by 1–15% and 1–5%, respectively, under 2 °C warming (FIG. 3g–j). The expansion of semi-arid regions mainly occurs in the Mediterranean, southern Africa and North and South Americas, while the expansion of arid regions occurs in south-western Africa²⁴, predominately by encroaching into neighbouring less arid zones (FIG. 3g–j). The spatial extent of dry sub-humid regions, in contrast, is projected to slightly decrease through fast converting to drier climates (FIG. 3g). When accounting for CO₂ impacts on surface hydraulic resistance in the definition of AI ($f_{\text{AI,CO}_2}$), a qualitatively similar expansion of global drylands is found, although the expansion rate is lower for almost all the continents (FIG. 3i), as also evident in the present climate.

For alternative interpretations of dryland extent, projected changes generally exhibit similarities in sign to those found for the historical period. Specifically, under RCP4.5, ESMs project that historical trends of strongly increasing f_{atm} , slightly increasing f_{soil} and strongly decreasing f_{veg} will continue to the end of the twenty-first century (FIG. 2). In more detail, f_{atm} is anticipated to experience rapid expansion across all the continents, exceeding 10% of total area when warming is higher than 2 °C (FIG. 3a). This widespread atmospheric drying trend is also evidenced by the progressive expansion of more arid dryland subcategories into previously less arid regions (FIG. 3b–e). Similarly, f_{soil} is also projected to increase throughout the twenty-first century across all the continents except for northern Africa (FIG. 3k), with the largest fractional increase occurring in semi-arid regions (FIG. 3l–o). One notable change is that, although f_{hyd} historically shows a slight increasing trend, this metric is projected to be reversed to a future decreasing trend under RCP4.5 (FIG. 2i; TABLE 1). However, the projected future f_{hyd} change is regionally heterogeneous, with slight expansions anticipated in North America, South America and southern Africa, but slight reductions in Eurasia, Australia and northern Africa (FIG. 3p).

Following a similar trajectory to historical changes, the projected future f_{veg} shows a widespread and persistent decreasing trend (FIGS 2j, 3u), spanning from

–6.6% in southern Africa to –25.3% in North America by the 2090s (2091–2100) relative to 1961–1990 (FIG. 3u, z). Under the 2 °C warming scenario, f_{veg} is projected to decrease by $10.7 \pm 3.3\%$ globally relative to the 1961–1990 baseline (FIG. 3u). Vegetation in many of the historical transitional zones between dry and wet climates (defined as sub-humid or semi-arid), such as in temperate central North America and north-eastern China, is expected to move from arid-climate-adapted to humid-climate-adapted (FIG. 3z). All of the four subcategories of dryland vegetation are expected to decrease in area, except for semi-arid regions in Australia and Eurasia, where more arid areas are moving into this vegetation-defined semi-arid subcategory than those moving out of semi-arid areas to dry sub-humid areas due to the stronger greening trend in arid ecosystems (FIG. 3v–y).

CMIP6-projected changes. Adding to the well-established CMIP5 ensembles of simulations, newer simulations archived in Phase 6 of the CMIP (CMIP6)⁷⁴ offer higher spatial resolution, improved physical parameterizations and the inclusion of additional Earth system processes^{74,75}.

Under SSP2-RCP4.5 — a scenario of intermediate emission and continuing historical socio-economic activities — CMIP6 ESMs project a persistent expansion of AI-based drylands over the twenty-first century at an average rate of $0.28 \pm 0.02\%$ per decade ($p < 0.05$), driven by a positive VPD trend of 0.030 ± 0.001 kPa per decade (Supplementary Table 5; Supplementary Fig. 5). Owing to the greater growth of atmospheric CO₂ forcing in SSP2-RCP4.5, this rate of dryland expansion is larger than the $0.20 \pm 0.02\%$ per decade ($p < 0.01$) projected by CMIP5 under RCP4.5 (TABLE 1).

When examining hydrological changes, CMIP6 ESMs show a significant increase in both total-column soil moisture and surface runoff over 2015–2100: $0.05 \pm 0.01\%$ per decade ($p < 0.01$) and 0.03 ± 0.01 mm per year ($p < 0.01$), respectively (Supplementary Fig. 5c,d). Despite the overall surface wetting, changes are spatially heterogeneous and regional hotspots of strong drying occur in the Mediterranean, western North America, southern Africa and Australia⁶⁰. The overall wetting projected by CMIP6 ESMs is in contrast to the overall drying (or insignificant change) projected by CMIP5 (FIG. 2c,d), which might be attributed to precipitation enhancements in the Middle East and northern Africa⁶⁰, and higher surface resistance under elevated CO₂ (REF.⁴⁵) in the former. A caveat is that such CO₂ regulation of hydrological dynamics has not been explicitly considered in some CMIP models because they represent a class of atmosphere–ocean general circulation model, without simulating dynamic vegetation. Hence, uncertainties exist in previous CMIP-based assessments of future hydrological changes, as atmosphere–ocean general circulation models are commonly included^{45,60,63}. For dryland ecosystem responses, CMIP6 ESMs also project that the historical trends of ecosystem greening and enhanced productivity will continue into the near future, similar to CMIP5 ESMs.

Model projections from CMIP5, therefore, broadly show a persistence of contemporary trends of dryland

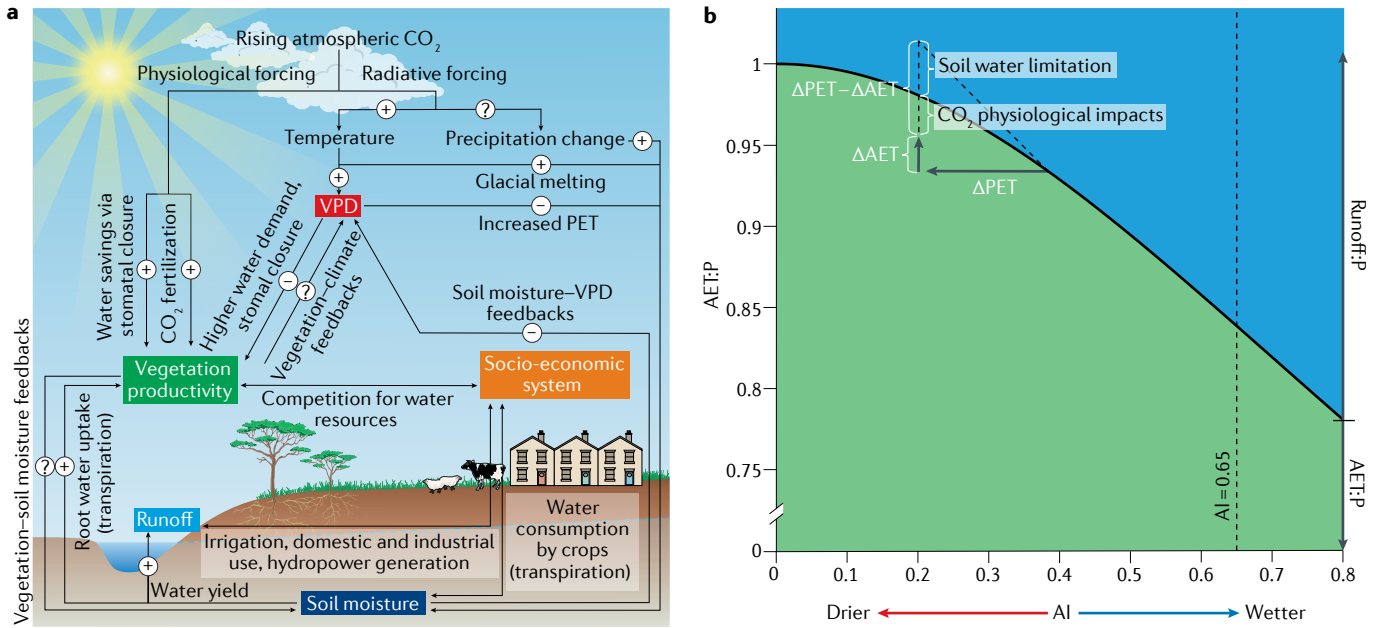


Fig. 4 | Physical and physiological mechanisms for dryland aridity changes. **a** | Schematic representation of processes underlying aridity changes of the atmospheric, hydrological, ecological and socio-economic systems, under warming and rising atmospheric CO₂. Circled symbols of ‘-’, ‘+’ and ‘?’ represent a negative, positive or potentially unknown sign of impact, respectively. **b** | Mechanisms for the shifting partitioning of precipitation between actual evapotranspiration (AET) and runoff under warming and elevated CO₂. The curve shows the Budyko framework^{173,174},

which links the partitioning of precipitation (P) into AET (green shaded area) and runoff (blue shaded area) to surface aridity level (defined by the aridity index, AI). The symbol ‘Δ’ denotes change of the corresponding quantity under warming and elevated CO₂. Under conditions of warming and decreasing AI values, the AET increase (vertical black arrow) cannot keep up with the potential evapotranspiration (PET) increase (horizontal black arrow), owing to the water limitations and the physiological regulations of plant water loss under elevated CO₂. VPD, vapour pressure deficit.

aridity changes throughout the twenty-first century. In particular, despite the continuously rising atmospheric dryness and soil moisture stress, dryland ecosystems are expected to continue greening. The divergent aridity changes over drylands with CMIP5 ESMs are also predicted by recently released CMIP6 simulations; however, these project a stronger atmospheric drying based on VPD and the AI, and a robust trend of land surface wetting (rather than drying or slight wetting based on CMIP5) assessed with soil moisture and runoff.

Mechanisms for dryland aridity changes

It is generally known that many land and atmospheric aridity processes, such as VPD, soil moisture and vegetation greenness, are essentially coupled over sub-seasonal to inter-annual timescales^{47,48,76} (FIG. 4a). However, over multi-decadal or longer timescales, highly divergent — and, in some instances, decoupled — trends of dryland aridity changes emerge, the size and direction of which are dependent on the chosen aridity metric. Specifically, as discussed, atmospheric aridity, characterized by water vapour and precipitation deficits, does not fully propagate to water deficits in the hydrosphere and the biosphere. This phenomenon is likely because each component of the coupled atmosphere–plant–hydrology system has a distinct and interactive response to rising atmospheric CO₂ and associated effects (FIG. 4a), and, thus, reveals different aspects of dryland aridity changes. In particular, accounting for the soil moisture constraints and leaf stomatal physiological response to rising CO₂ helps explain and reconcile the divergence in

aridity changes by different metrics to some extent, as will now be discussed.

Thermodynamic changes drive higher atmospheric demand for water.

Observed atmospheric drying — that is, rising VPD (FIG. 2a,f) — is generally accepted as a simple thermodynamic consequence of warming^{18,36}. The lack of surface moisture and evaporative cooling amplifies regional surface warming in drylands compared with humid lands and oceans². The higher temperatures augment the capacity of the air to hold more water vapour. However, the greater warming over land than oceans impedes the transport of moist air masses from oceans to the land, particularly in subtropical subsidence zones, making the increase of near-surface specific humidity over the land relatively small and insufficient to follow Clausius–Clapeyron scaling (~7% per °C)^{18,77,78}. The enlarged contrast between actual and saturated water vapour, that is, higher VPD, provides an explanation for the PET increase^{18,24,36}, which exceeds concurrent precipitation increases and, thus, causes reduced AI values (enhanced aridity) and the associated expansion of dryland extent^{10,18,24,25} (FIGS 2b,g,3f).

Furthermore, land surface processes also modulate atmospheric dryness through land–atmospheric feedbacks^{48,76} (FIG. 4a). For instance, warming-induced depletion of soil moisture attenuates evaporative cooling and elevates temperature (thus, also elevating VPD and PET), while simultaneously enhancing atmospheric stability and inhibiting cloud formation and precipitation generation⁷⁶. Soil moisture depletion also strengthens

the gradients of air humidity and pressure between drylands and surrounding humid regions, which promotes low-level moisture convergence and increases precipitation transported to global drylands⁷⁹. Jointly, these compensatory physical processes lead to an exacerbation of surface aridity characterized by decreased AI values⁷⁶.

Importantly, the explanation of dryland aridity changes with atmospheric thermodynamics and regional land–atmosphere interactions does not account for structural changes of large-scale atmospheric circulations. In particular, the Hadley circulation is essential for the development of subtropical dryland climates². Observational evidence has indicated a widening (or poleward expansion) of the subsiding branches of the Hadley circulation, as well as a strengthening of descending motion in the subtropics^{80,81}. These circulation changes suppress convective precipitation and reduce tropospheric humidity, hence, intensifying surface aridity in subtropical zones^{80,81}. However, uncertainties remain in changes of the Hadley circulation and associated climatic consequences, and they are not able to explain the observed overall increase in precipitation over subtropical lands². In addition, climate model projections of drier subtropics under future warmer climates contradict palaeoclimatic evidence of wetter subtropics in past warm periods⁸²; the wetter subtropics under past warm climates are suggested to co-occur with weakened (rather than present-day strengthened) subtropical subsidence of the Hadley circulation associated with weaker-than-present meridional sea-surface temperature gradients⁸².

Vegetation physiological responses to rising atmospheric CO₂. Assuming fixed or only small increases in precipitation, alongside no change in direct human consumption, available water resources (soil moisture and runoff) over the land will decrease. This reduction arises from anthropogenic-warming-enhanced evaporative losses, owing to heightened PET^{18,68,72,83}. However, changes in actual evapotranspiration (AET) are governed by more than the thermodynamics that determine PET. In particular, the thermodynamically driven growth in PET cannot translate into similar growth in AET over drylands, as the limited soil moisture supply strongly constrains the AET increase if precipitation remains steady^{84,85} (FIG. 4b). There is also growing evidence that vegetation physiological processes have a critical role in controlling AET and, thus, other hydrological fluxes^{45,86–89}. The different governing processes of PET and AET create a growing gap between them under rising atmospheric CO₂, which underlies the inconsistent changes between the AI (depending on PET changes) and other ecohydrological aridity measures (affected by AET by varying amounts) (FIG. 4b).

As atmospheric CO₂ increases, plant leaves partially close their stomata and reduce the amount of water loss through stomatal transpiration. This leaf-scale stomatal regulation is simultaneous with, and could be potentially counteracted by, changes in structural and functional attributes of plants, including enhanced photosynthesis⁹⁰, increased canopy leaf area³² and deepened rooting system⁹¹ (FIG. 4a). In particular, the expansion of foliage area induces extra water loss via leaf

transpiration and canopy evaporation of intercepted rainfall, while simultaneously decreasing evaporative water loss from the soil surface^{32,92}. As plant transpiration accounts for more than half of the land AET in dryland natural ecosystems⁹³, transpiration (rather than evaporation) responses to higher CO₂ will likely dominate the overall dryland AET changes in a CO₂-enriched world⁹⁴.

However, at least for the recent past (1948–2016), there is no consensus as to the net hydrological effect of plant physiological responses to higher CO₂, linked to uncertainties in the complex interactions and compensations among relevant biophysical processes^{19,95}. Under future scenarios with a much higher atmospheric CO₂ concentration (for instance, reaching a quadrupling of the pre-industrial CO₂ level), model projections generally agree on a net decrease of canopy-level transpiration and land AET after accounting for both stomatal regulation and foliage expansion^{45,86,87,89}. This physiological forcing of high atmospheric CO₂ on AET could even dominate over its radiative forcing in some less arid dryland areas with sizeable vegetation cover⁸⁷.

The plant physiological responses to elevated CO₂ can partly explain the divergent dryland aridity changes, simultaneously ameliorating ecohydrological water stress and increasing atmospheric dryness (Supplementary Figure 6). The stomatal regulation of transpiration under elevated CO₂ level can conserve water, which generally favours the partitioning of precipitation towards runoff and soil moisture^{45,86–88,94,96} (FIG. 4; Supplementary Figure 6). Vegetation growth of water-limited biomes, as for drylands, is more sensitive to soil moisture deficit than to atmospheric moisture deficit^{97,98}, and, hence, CO₂-driven water saving can offset the higher water demand driven by a warmer atmosphere. Such CO₂-driven water saving is sufficient to ameliorate water limitations for photosynthesis in semi-arid grasslands, as confirmed by manipulative free-air CO₂-enrichment experiments^{99–101} and factorial simulations with DGVMs (BOX 2). This water-saving mechanism, in concert with CO₂-induced stimulation of photosynthesis, longer growing seasons and attenuated soil moisture stress at places with increased precipitation, translates to extra carbon gain and enhanced growth, and moves the dryland ecosystem to a new hydro-ecological equilibrium^{28,102,103}.

Meanwhile, the physiologically induced transpiration decrease also feeds back to surface climate through reduced evaporative cooling, thus, contributing to the warming¹⁰⁴ and relative drying of the near-surface air, which is reflected in enhanced VPD^{76,89} (Supplementary Figure 6). The CO₂ physiological effect on hydrology and surface climate, as previously discussed, is small in extremely arid areas, but in semi-arid and sub-humid areas, this effect is substantially larger and even comparable with that in humid areas (Supplementary Figure 6).

Uncertainties in current understanding of CO₂ physiological impacts. Large uncertainties exist in the estimation of CO₂ physiological impacts on dryland ecohydrological changes. Many studies of CO₂ physiological forcing are based only on numerical simulations that depend heavily on model parameterization schemes of

Box 2 | Characterizing CO₂ physiological impacts on dryland productivity

Owing to the confounding effect of climate change, it is difficult to quantify dryland ecosystem responses to elevated CO₂ with empirical statistical models and historical records. Dynamic global vegetation models (DGVMs) (Supplementary Table 2) participating in the “Trends in net land-atmosphere carbon exchange” (TRENDY; Supplementary Methods) project enable the quantitative characterization of CO₂ physiological forcings, for example, using the simulation S1 forced by varying CO₂ but fixed climate¹⁷⁹. Higher CO₂ enhances gross primary production (GPP) through two parallel physiological processes: the direct CO₂ fertilization effect that enhances productivity while simultaneously consumes more water and the indirect physiological effect, which reduces stomatal conductance and, thus, conserves water for additional carbon uptake. The following analysis extracts contributions of the two counteracting mechanisms to dryland GPP changes.

GPP can be represented as the product of canopy-scale transpiration (E_t) and canopy-scale water-use efficiency (WUE_c):

$$GPP = E_t \cdot WUE_c \tag{2}$$

By applying a differential transformation, fractional GPP changes are presented as:

$$\frac{dGPP}{GPP_0} = \frac{dE_t}{E_{t0}} + \frac{dWUE_c}{WUE_{c0}} \tag{3}$$

where the subscript ‘0’ denotes the value for a baseline period (1948–1957). For a fixed precipitation amount, the strong water limitation for dryland ecosystems determines that E_t is approximately conserved²⁸. For example, DGVMs (in the simulation forced by both varying CO₂ and climate) estimate a slight E_t increase by +0.9% from 1948–1957 to 2007–2016. Hence, WUE_c changes can almost fully explain the CO₂-driven increase of dryland GPP.

Warm and arid ecosystems often have simple above-ground structure, typically with leaf area index (L) less than unity. This means that an increase in L would usually capture, linearly, more light and, thus, be proportionally related to enhanced transpiration and productivity^{28,180}. Hence, leaf-level CO₂ assimilation (A) and water loss ($E_{t,l}$) can be approximated as GPP and transpiration per unit leaf area (Eq. 4). Under this assumption, WUE_c can be directly scaled from the WUE of individual leaves (WUE_l) (Eq. 5), as robustly supported by field experiments^{181,182}. Hence:

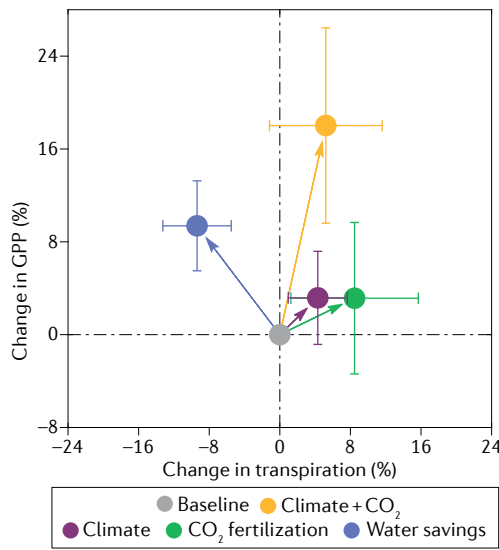
$$E_t = \int E_{t,l} \approx E_{t,l}L; GPP = \int A \approx AL \tag{4}$$

$$WUE_c \approx WUE_l = \frac{A}{E_{t,l}} \tag{5}$$

By integrating Eqs. 3–5 to Eq. 6, fractional changes of WUE_c can be separated into contributions from changes of leaf-level carbon and water fluxes:

$$\frac{dWUE_c}{WUE_{c0}} \approx \frac{dWUE_l}{WUE_{l0}} = \frac{dA}{A} + \left(-\frac{dE_{t,l}}{E_{t,l0}} \right) \tag{6}$$

Equation 6 enables a disaggregation of the two physiological responses. The first term (dA/A_0) can be interpreted as the leaf-scale CO₂ fertilization effect and the second term ($-dE_{t,l}/E_{t,l0}$) as the leaf-scale CO₂ water-saving effect. By integrating these equations and DGVM simulations, the water-saving effect is estimated to contribute 52% of the dryland GPP increase from 1948–1957 to 2007–2016, much higher than the effect of CO₂ fertilization (18%) and climate change (18%).



ecosystem response^{45,86–89,105}. For example, some experimental studies suggest that the capacity of dryland plants to optimize their carbon sequestration and water utilization under higher CO₂ is limited, owing to the dominant role of soil moisture limitations in controlling plant physiological responses to CO₂ (REFS^{106,107}) and possible nutrient depletion¹⁰⁸. Such processes are not yet sufficiently understood, and, consequently, errors in their parameterization in DGVMs might be substantial³². At present, more observational and experimental techniques, such as leaf gas exchange, stable isotope discrimination and eddy covariance measurement, are now implemented to investigate plant water use^{109–111}. Yet, these approaches are rarely applied to the scale of ecosystem or river basin, due to the substantial discrepancy at different spatial and temporal scales¹⁰⁹ or the short temporal coverage that precludes the detection of slowly evolving CO₂ impacts.

ESMs project that dryland vegetation greening will continue to benefit from future atmospheric CO₂ enrichment (REFS^{32,103}). However, as temperature continues to increase, whether the positive CO₂ physiological impact on vegetation will persist remains an open question. Temperature and precipitation feedbacks from CO₂-induced stomatal closure and AET reduction can amplify the risk of surface heat stress^{112–114}, which might offset, or even reverse, the positive effect of water stress relief. More importantly, with increasing warming, plants could need to keep stomata open to cool their leaves from irreversible heat damage, despite elevated CO₂ allowing for reduced stomatal aperture to maintain the same or even raised photosynthetic rate^{115,116}. This required stomatal opening could be increasingly important for dryland biomes as temperatures rise, since current temperatures appear to be near or above the optimum for photosynthesis¹¹⁷. Future research needs to place more emphasis on understanding possible non-linearities or tipping points of critical transitions^{50,51} in dryland ecosystem responses to future global warming and improving their representations in process-based models. In particular, long-term manipulative field experiments will be useful to better characterize any non-linear features of plant responses and assess dangerous levels of future warming over drylands^{118,119}.

Towards a human-dominated dryland

Earth is now in the Anthropocene era¹²⁰, when humans are playing a central or even dominant role in shaping terrestrial greenness patterns and modifying regional hydrological cycles^{62,121–123}. Direct human impacts are, in some instances, more substantial than natural factors and indirect human forcing via climate change. Global drylands are currently experiencing the fastest population growth in the world¹²⁴, which makes the already fragile dryland environment even more vulnerable to water scarcity. Therefore, human freshwater use, which is heavily influenced by demographical, social, economic and technological factors¹²⁵, must be incorporated in dryland aridity assessment and predictions. Global hydrological models (GHMs), forced by varying scenarios of both historical and future socio-economic

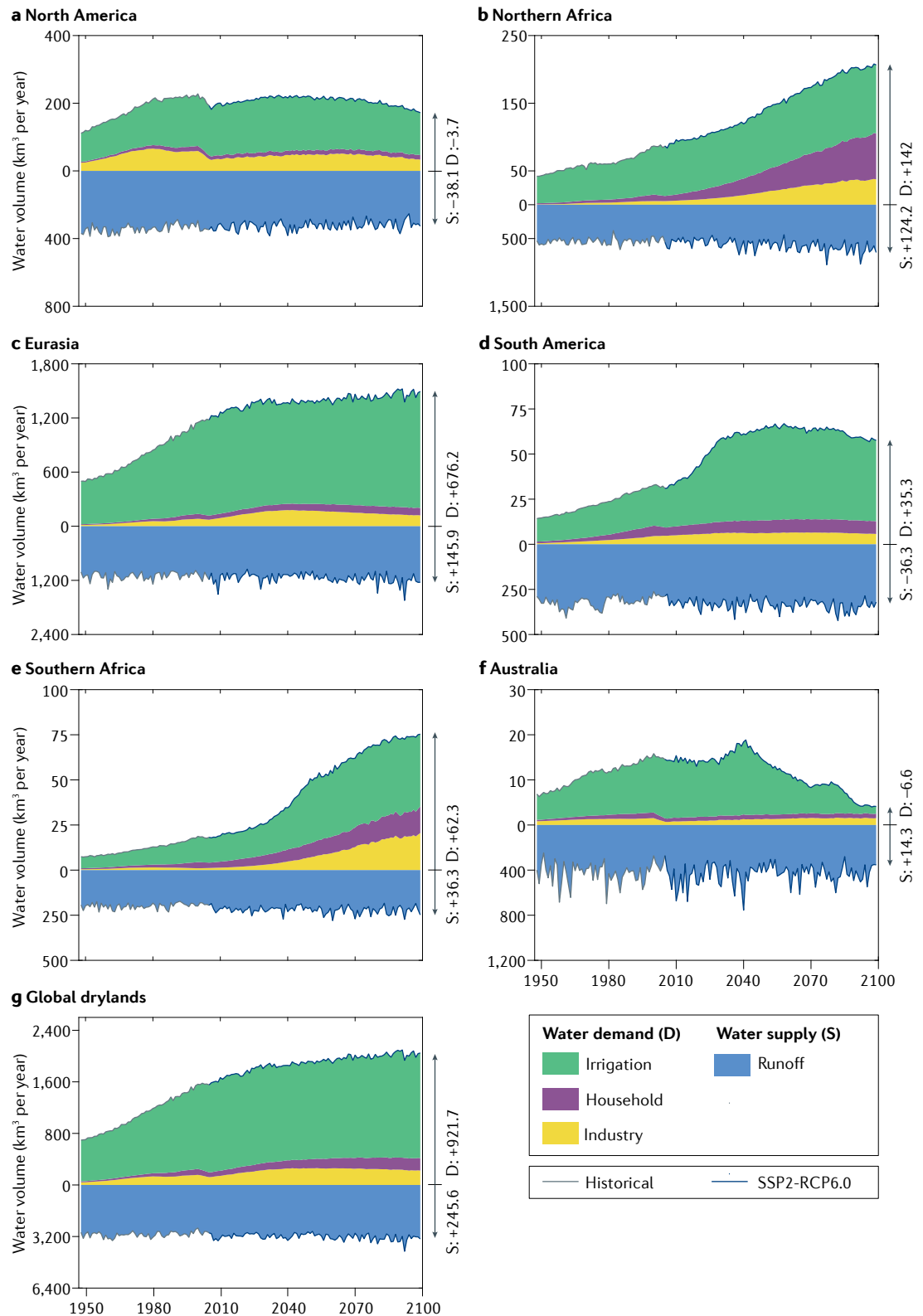


Fig. 5 | Dryland anthropogenic water stress under climatic and socio-economic changes. Historical and future changes of total anthropogenic water for North America (panel **a**), northern Africa (panel **b**), Eurasia (panel **c**), South America (panel **d**), southern Africa (panel **e**), Australia (panel **f**) and global drylands (panel **g**); for map of regions, see FIG. 3z. The water demand (D) is presented as a sum of agricultural, domestic and industrial water withdrawal, and the water supply (S) is mainly surface runoff. The time series are derived from the ensemble mean of three global hydrological models (global hydrological models, including H08, MATSIRO and LPJmL) under the SSP2-RCP6.0 scenario. Arrows show the amount of D and S during the 2090s, with the numbers on the right showing the relative changes to the 1961–1990 baseline.

factors and greenhouse gas emissions (Supplementary Methods), are available for such assessments^{126,127} (FIG. 5).

GHMs indicate that, since the 1950s, rapid population growth and economic development has increased human water demand in drylands by approximately 200% (FIG. 5g). Furthermore, this rapid increase in human water demand is expected to increase by ~270% (on the baseline of the 1950s) by the 2090s under SSP2-RCP6.0, a no-mitigation emission pathway (FIG. 5g). Agricultural irrigation contributes the greatest overall increase of dryland water use for all the continents, for both historical and future periods^{128,129} (FIG. 5). In addition, industrial and domestic water demands are also projected to increase substantially, especially in African drylands (FIG. 5b,e).

However, GHMs forced with changing socio-economic factors do not project monotonically increasing human water demand throughout the twenty-first century (FIG. 5g). These models estimate an increase in water demand consistently for all the continents before the 2030s. After the 2030s, however, regional projections diverge, with a continuous rise in Africa (FIG. 5b,e), a levelling off in Eurasia and South America (FIG. 5c,d) and a decline in North America and Australia (FIG. 5a,f). Given the relatively small water supply changes of surface runoff, the rapid augmentation of water needs in Eurasia, South America and, in particular, Africa will exacerbate societal water scarcity (the gap between water demand and supply) in those regions (FIG. 5). This geographical divergence also highlights a major concern that many of the poorest regions, with very limited access to financial and technological resources, are more likely to be exposed to high pressures of water scarcity in the future. Importantly, there is accumulating experimental evidence that crop plants can use water more efficiently under rising atmospheric CO₂ (REFS^{130–132}). The CO₂ physiological effects can partly, though not fully, offset the anticipated increase of agricultural water consumption, and, thus, alleviate the adverse impact of surface warming and drying to some extent^{130–132}.

The rapidly growing freshwater demands might not be sustainable, and have already imprinted noticeable footprints on local to global hydrological cycles. Agricultural expansion and intensification, though contributing to regional greening and increased vegetation productivity in many places^{32,73}, are often accompanied with excessive withdrawal of surface waters (mainly runoff) and overextraction of groundwater storage^{128,133,134}. In particular, gravity-based remote sensing demonstrates that groundwater levels in India¹³⁵, the North China Plain¹³⁶ and western USA⁸³ are falling at an alarming rate. Groundwater extraction for agricultural irrigation is now exceeding the natural recharge rate in these regions, recognized as the main cause for the observed decline in groundwater levels^{128,134,135}. Many plant species in arid and semi-arid areas depend on shallow groundwater for survival, particularly during dry seasons when other water sources are largely unavailable^{137,138}. Therefore, such unsustainable groundwater depletion also poses a significant threat to the health of dryland natural ecosystems^{138,139}.

In addition to the direct extraction of water resources, other human land-use management practices, such as afforestation (or reforestation), deforestation, overgrazing and urbanization, also leave remarkable imprints on dryland ecohydrological systems. For example, while contributing to halting desertification and increasing carbon storage^{140,141}, large-scale ecological restoration programmes implemented in semi-arid or sub-humid North and West China have caused extra evaporative water loss and a related significant decrease in regional runoff and terrestrial water storage^{140,142,143}. The faster return of water to the atmosphere means that less water is available for other socio-economic needs. Meanwhile, overgrazing is also a significant anthropogenic factor contributing to grassland deterioration and even the shift of dominant vegetation types, potentially disturbing local hydrological cycles. This deterioration is a key environmental problem faced by regions economically dependent on livestock, such as Mongolia, central Eurasia, Latin America and sub-Saharan Africa^{144,145}. By removing protective plant cover and by livestock trampling, overgrazing may cause the compaction of soils, reducing infiltration and accelerating runoff and soil erosion¹⁴⁶.

More efficient water resource management measures can help to cope with the increasing water crisis, with substantial co-benefits for the sustainability of the coupled dryland social-ecological system. First, taking advantage of the increasing crop water-use efficiency under elevated CO₂ (REFS^{131,132}), it might be possible to gradually reduce irrigation water usage per unit area of agricultural land. This irrigation reduction is complementary to other agricultural water management approaches, such as rainwater harvesting, precise irrigation and improved irrigation infrastructure. Second, there is growing attention placed on the benefits of future forestry practices, and especially afforestation as a potential solution to partially offset CO₂ emissions^{147,148}. Afforestation programmes in dryland regions need to use locally adapted and water-efficient indigenous species to avoid unnecessary evaporative water losses¹⁴⁹. Careful evaluation is also required of the land carrying capacity to support anticipated plant growth^{140,150}. Third, policy decisions may gain from incorporating water-relevant ecological information from the ever-expanding near-real-time data streams from space. For example, the incorporation of satellite monitoring of gross primary production and chlorophyll fluorescence into drought early-warning systems¹⁵¹ can help guide governments to take anticipatory mitigation actions in preserving farming livelihoods and food security.

New water conservation technologies are also helpful to safeguard dryland water and food security. For example, improved agricultural biotechnology is expected to breed more drought-tolerant and/or salt-tolerant, water-efficient and more productive cereal and forage crops¹⁵². Such advances will simultaneously increase agricultural production and reduce water usage. Modelling evidence also suggests that the adoption of new technologies, such as developing renewable energy and recirculating dry-cooling systems in

electricity generation, could lower ~32% of global water requirements by 2100 under the SSP5 scenario (REF. 153). Nonetheless, the effectiveness of such technological innovations for drylands depends on their transfer to and implementation by some of the world's poorest countries.

Summary and future perspectives

Dryland ecosystems are a pivotal part of the Earth system and their sustainability is critical both locally and for our shared societal future. While water is the central component in defining dryland social-ecological systems,

aridity in drylands is tightly interconnected with climate, vegetation and humans, all of which vary over different spatio-temporal scales. Whilst numerous studies define dryland changes with a broad range of metrics, these often generate highly conflicting conclusions. Such discrepancies lead to less trust in projections of environmental change and can preclude the accurate determination of dangerous thresholds of climate alteration.

This Review leverages comprehensive strands of data and research pertaining to drylands for a holistic overview of their global changes. By viewing the emerging aridity changes as adjusting attributes of a coupled

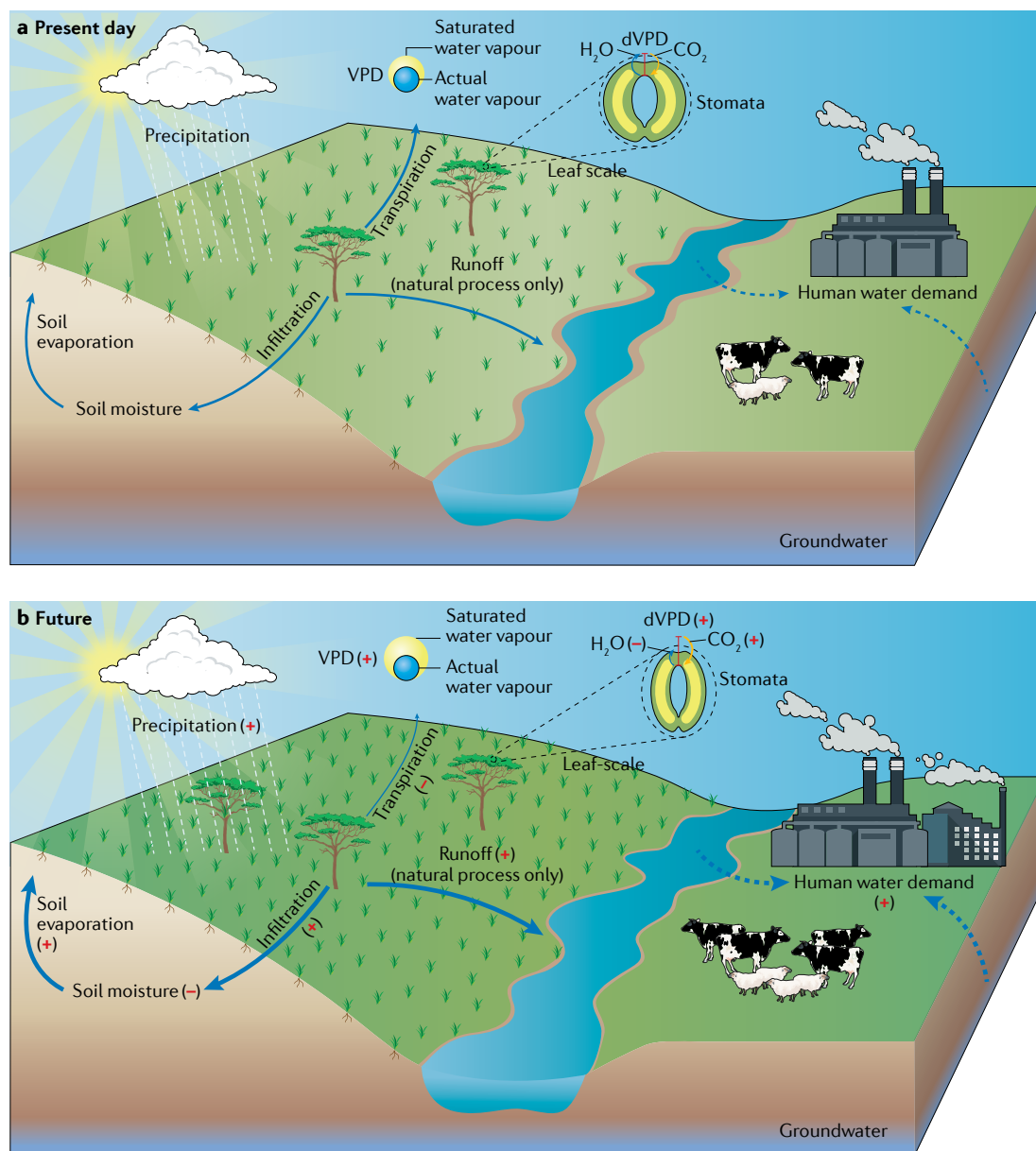


Fig. 6 | Conceptual diagram of future dryland aridity changes. Present-day (panel a) versus future (panel b) aridity conditions of the atmospheric, hydrological, ecological and socio-economic systems over drylands. Future changes of dryland ecohydrological variables are based on CMIP5 simulations, without accounting for direct human interference. In panel b, red symbols of '+' and '-' in brackets represent an overall increase and decrease, respectively, in the corresponding quantity, relative to its present-day level. Note that the potential spatial heterogeneity of ecohydrological changes is not illustrated. The anticipated water demand changes (dashed arrows) of the human society are based on global hydrological model simulations. VPD, vapour pressure deficit.

atmosphere–ecohydrology–human system, we provide a cohesive picture of recent, ongoing and future dryland changes (FIG. 6). At short timescales such as daily to inter-annual, aridity changes are primarily governed by climate variability, regardless of the metric used. Yet, over longer decade to century timescales, the CO₂ physiological effect is likely a more important driver for vegetation-related aridity changes, with important feedbacks to local and regional hydrological cycles (FIG. 6). The role of plant physiological mechanisms in ameliorating plant water stress and fostering plant growth will become even more important and helpful, against a backdrop of rising water and food demands by the rapidly growing population (FIG. 6).

Although the mechanistic understanding of surface aridity changes is for the recent past and the near future, it might also have broader implications beyond the contemporary timescale. In particular, the CO₂ physiological forcing provides a useful mechanism for explaining the warmer-and-greener association observed over the geological timescale. Ice core and pollen-based hydroclimate reconstructions suggest that warmer interglacial periods (for example, the Pliocene period with atmospheric CO₂ concentration of 350–450 ppm, as comparable with the current CO₂ level) are often associated with lower dust levels (often indicative of a wetter land surface)¹⁵⁴ and generally higher vegetation cover, compared with colder glacial periods (for example, the Last Glacial Maximum with atmospheric CO₂ concentration of ~190 ppm)^{155–157}. This phenomenon again contradicts with model-estimated lower AI values (land surface drying) for warmer periods¹⁵⁸, but does agree with present-day trends for increasing vegetation cover. That is, analysis from the current climate suggesting that the physiological influence of higher CO₂ levels in warmer periods shapes the surface water cycle and prevents the expansion of arid and semi-arid ecosystems, and this present-day process has presumably operated throughout the geological timescale. Decreased dust deposition in warmer periods does not, however, necessarily imply a wetter land surface, owing to potential confounding factors, such as changes in large-scale circulation patterns⁸², wind speed, aerosol concentrations and the likelihood that less dusty air is, itself, a result of higher vegetation cover^{63,154}.

Looking forward, we identify several remaining knowledge gaps as priorities for future research and policy decisions. Aridity, calculated as a long-term but changing average state of water scarcity, cannot represent all aspects of the societally relevant hydrological responses expected for future climatic states. Future research needs to prioritize the understanding of possible enhanced risk posed by short-term hydroclimatic anomalies and how ecosystems subsequently respond and adapt to such climate perturbations.

As the climate gets warmer, there is substantial evidence of increasing chances of more frequent and severe climate extremes, particularly droughts^{107,159–161}. Extreme dry events can trigger detrimental damage to the fragile dryland ecosystems, including raised mortality levels and enhanced fire risks^{162–164}. As one of the most fire-prone ecosystems, drylands account for

more than 80% of global wildfires, with massive losses of plant biomass and soil nutrients^{165,166}. Observational evidence shows widespread woody encroachment in subtropical savannas associated with decreased burned areas and fire return intervals during 1997–2016 (REF.¹⁶⁷). Contrary to the observed downward trends of historical records, current fire models usually project rising risks of fire disturbances under future climate change, yet, with a large spread of probabilities^{166,168}. The impact of future shifting fire regimes on dryland ecosystem–hydrology changes is, thus, still largely uncertain. However, dryland vegetation is also highly resilient and can often recover quickly from past disturbances¹⁶⁹, despite possible increasing risks from droughts and fires. The high resilience and fast recovery might represent a key mechanism for the adaptation of dryland vegetation to past and future climate change, and can additionally contribute to the differences noted between changes of vegetation aridity and those of other aridity indicators.

Global drylands also encompass a diverse range of regions, cultures and ecosystems, resulting in regional divergence in their aridity changes and associated impacts. This divergence implies highly regionalized challenges in meeting the societal and ecosystem needs of water resources³. Targeted regional assessments of dryland aridity changes will better inform effective mitigation actions if tailored to different specific localized needs.

There additionally remain challenges to observe and model accurately long-term changes of surface aridity and water resources^{159,170,171}. Field measurements and experiments remain scarce in drylands, and, at present, datasets are often too short to provide definitive answers on the long-term effects of CO₂ fertilization and stomatal behaviour. The scarcity of data prevents characterizing any potential non-linear responses as atmospheric CO₂ concentrations rise even higher. Thus, there is a pressing need for future efforts to build more extensive and high-quality dryland observation networks that operate over a range of spatial scales and substantial periods of time. Yet, even for measurements that are available, there needs to be more far-reaching integrated analyses of emerging space and ground-based measurements, such as eddy covariance, FACE experiments, plant functional traits and tree-ring chronologies, to provide a more complete mechanistic understanding of ongoing land surface processes. Moreover, future hydrological models must treat vegetation as a dynamic component, and explicitly consider the feedbacks of its structural and physiological changes to other key water-cycle components. Current models generate substantial uncertainties in projected trajectories of dryland water resource availability and requirements. Constraining such uncertainties requires refining the representation of the complex interactions between the climate, hydrology, ecosystems and humans. An improved predictive capability will support policymaking to achieve sustainable management of global drylands, to better service different societal and ecosystem needs in a warmer and CO₂-enriched world.

1. Reynolds, J. F. et al. Global desertification: building a science for dryland development. *Science* **316**, 847–851 (2007).
2. Huang, J. et al. Dryland climate change: recent progress and challenges. *Rev. Geophys.* **55**, 719–778 (2017).
3. Intergovernmental Panel on Climate Change (IPCC). *Climate Change and Land: An IPCC Special Report on Climate Change, Desertification, Land Degradation, Sustainable Land Management, Food Security, and Greenhouse Gas Fluxes in Terrestrial Ecosystems* (eds Akhtar-Schuster, M., Diouech, F. & Sankaran, M.) Ch. 3 (IPCC, Cambridge Univ. Press, 2019).
4. Právilie, R. Drylands extent and environmental issues. A global approach. *Earth Sci. Rev.* **161**, 259–278 (2016).
5. D'Odorico, P., Bhattachan, A., Davis, K. F., Ravi, S. & Runyan, C. W. Global desertification: drivers and feedbacks. *Adv. Water Resour.* **51**, 326–344 (2013).
6. Ahlström, A. et al. The dominant role of semi-arid ecosystems in the trend and variability of the land CO₂ sink. *Science* **348**, 895–899 (2015).
Highlights the critical role of drylands in the global carbon budget by demonstrating that semi-arid ecosystems dominate the inter-annual variability and the increasing trend of global terrestrial carbon sink.
7. Maestre, F. T. et al. Plant species richness and ecosystem multifunctionality in global drylands. *Science* **335**, 214–218 (2012).
8. Millennium Ecosystem Assessment. *Ecosystems and Human Well-Being: Desertification Synthesis* (World Resources Institute, 2005).
9. El-Beltagy, A. & Madkour, M. Impact of climate change on arid lands agriculture. *Agric. Food Secur.* **1**, 3 (2012).
10. Huang, J., Yu, H., Guan, X., Wang, G. & Guo, R. Accelerated dryland expansion under climate change. *Nat. Clim. Change* **6**, 166–171 (2016).
11. Cook, K. H. & Vizy, E. K. Detection and analysis of an amplified warming of the Sahara Desert. *J. Clim.* **28**, 6560–6580 (2015).
12. Zhou, L., Chen, H. & Dai, Y. Stronger warming amplification over drier ecoregions observed since 1979. *Environ. Res. Lett.* **10**, 064012 (2015).
13. Fu, B. et al. The Global-DEP conceptual framework — research on dryland ecosystems to promote sustainability. *Curr. Opin. Environ. Sustain.* **48**, 17–28 (2020).
Proposes a conceptual framework that aims to facilitate actionable pathways towards sustainable development of global dryland socio-ecological systems.
14. Larigauderie, A. & Mooney, H. A. The Intergovernmental science-policy Platform on Biodiversity and Ecosystem Services: moving a step closer to an IPCC-like mechanism for biodiversity. *Curr. Opin. Environ. Sustain.* **2**, 9–14 (2010).
15. Convention on Biological Diversity. *Aichi Biodiversity Targets* <http://www.cbd.int/sp/targets/default.shtml> (2020).
16. United Nations. *Transforming Our World: The 2030 Agenda for Sustainable Development* (United Nations General Assembly, 2015).
17. Park, C.-E. et al. Keeping global warming within 1.5 °C constrains emergence of aridification. *Nat. Clim. Change* **8**, 70–74 (2018).
18. Sherwood, S. & Fu, Q. A drier future? *Science* **343**, 737–739 (2014).
19. Ukkola, A. M. et al. Reduced streamflow in water-stressed climates consistent with CO₂ effects on vegetation. *Nat. Clim. Change* **6**, 75–78 (2015).
20. Wang, J. et al. Recent global decline in endorheic basin water storages. *Nat. Geosci.* **11**, 926–932 (2018).
Provides observational evidence for widespread loss of terrestrial water storage over global endorheic basins during 2002–2016 from climate variability and human water extractions.
21. Scheff, J. & Frierson, D. M. W. Terrestrial aridity and its response to greenhouse warming across CMIP5 climate models. *J. Clim.* **28**, 5583–5600 (2015).
22. Koutroulis, A. G. Dryland changes under different levels of global warming. *Sci. Total Environ.* **655**, 482–511 (2019).
23. Schewe, J. et al. Multimodel assessment of water scarcity under climate change. *Proc. Natl Acad. Sci. USA* **111**, 3245–3250 (2014).
24. Feng, S. & Fu, Q. Expansion of global drylands under a warming climate. *Atmos. Chem. Phys. Discuss.* **13**, 14637–14665 (2013).
25. Cook, B. I., Smerdon, J. E., Seager, R. & Coats, S. Global warming and 21st century drying. *Clim. Dyn.* **43**, 2607–2627 (2014).
26. Zhang, P. et al. Abrupt shift to hotter and drier climate over inner East Asia beyond the tipping point. *Science* **370**, 1095–1099 (2020).
27. He, B., Wang, S., Guo, L. & Wu, X. Aridity change and its correlation with greening over drylands. *Agric. For. Meteorol.* **278**, 107663 (2019).
28. Donohue, R. J., Roderick, M. L., McVicar, T. R. & Farquhar, G. D. Impact of CO₂ fertilization on maximum foliage cover across the globe's warm, arid environments. *Geophys. Res. Lett.* **40**, 3031–3035 (2013).
Reveals widespread greening in global arid regions despite warming, and provides quantitative theoretical evidence linking this greening pattern with elevated CO₂.
29. Fensholt, R. et al. Greenness in semi-arid areas across the globe 1981–2007 — an Earth Observing Satellite based analysis of trends and drivers. *Remote Sens. Environ.* **121**, 144–158 (2012).
30. Andela, N., Liu, Y. Y., van Dijk, A. I. J. M., de Jeu, R. A. M. & McVicar, T. R. Global changes in dryland vegetation dynamics (1988–2008) assessed by satellite remote sensing: comparing a new passive microwave vegetation density record with reflective greenness data. *Biogeosciences* **10**, 6657–6676 (2013).
31. Zhu, Z. et al. Greening of the Earth and its drivers. *Nat. Clim. Change* **6**, 791–795 (2016).
32. Piao, S. et al. Characteristics, drivers and feedbacks of global greening. *Nat. Rev. Earth Environ.* **1**, 14–27 (2020).
33. Beck, H. E. et al. Global evaluation of four AVHRR–NDVI data sets: Intercomparison and assessment against Landsat imagery. *Remote Sens. Environ.* **115**, 2547–2563 (2011).
34. United Nations World Water Assessment Programme. *The United Nations World Water Development Report 2015: Water for a Sustainable World* (UNESCO, 2015).
35. Wang, L. et al. Dryland ecophysiology and climate change: critical issues and technical advances. *Hydrol. Earth Syst. Sci.* **16**, 2585–2603 (2012).
36. Roderick, M. L., Greve, P. & Farquhar, G. D. On the assessment of aridity with changes in atmospheric CO₂. *Water Resour. Res.* **51**, 5450–5463 (2015).
A comprehensive summary of contradictory viewpoints of 'warmer is more arid' versus 'warmer is less arid' that arise from different interpretations of aridity changes, and provides a road map for reconciling such disparities.
37. Swann, A. L. S. Plants and drought in a changing climate. *Curr. Clim. Change Rep.* **4**, 192–201 (2018).
38. Greve, P. et al. Global assessment of trends in wetting and drying over land. *Nat. Geosci.* **7**, 716–721 (2014).
39. Smith, W. K. et al. Remote sensing of dryland ecosystem structure and function: progress, challenges, and opportunities. *Remote Sens. Environ.* **233**, 111401 (2019).
40. Greve, P., Roderick, M. L., Ukkola, A. M. & Wada, Y. The aridity index under global warming. *Environ. Res. Lett.* **14**, 124006 (2019).
41. Huang, J., Yu, H., Dai, A., Wei, Y. & Kang, L. Drylands face potential threat under 2 °C global warming target. *Nat. Clim. Change* **7**, 417–422 (2017).
42. Middleton, N. & Thomas, D. *World Atlas of Desertification* (Arnold, 1997).
43. Fu, Q. & Feng, S. Responses of terrestrial aridity to global warming. *J. Geophys. Res. Atmos.* **119**, 7863–7875 (2014).
44. Yang, Y. et al. Disconnection between trends of atmospheric drying and continental runoff. *Water Resour. Res.* **54**, 4700–4713 (2018).
45. Yang, Y., Roderick, M. L., Zhang, S., McVicar, T. R. & Donohue, R. J. Hydrologic implications of vegetation response to elevated CO₂ in climate projections. *Nat. Clim. Change* **9**, 44–48 (2019).
46. Greve, P., Roderick, M. L. & Seneviratne, S. I. Simulated changes in aridity from the last glacial maximum to 4xCO₂. *Environ. Res. Lett.* **12**, 114021 (2017).
47. Yuan, W. et al. Increased atmospheric vapor pressure deficit reduces global vegetation growth. *Sci. Adv.* **5**, eaax1596 (2019).
48. Zhou, S. et al. Land–atmosphere feedbacks exacerbate concurrent soil drought and atmospheric aridity. *Proc. Natl Acad. Sci. USA* **116**, 18848–18853 (2019).
49. Grossiord, C. et al. Plant responses to rising vapor pressure deficit. *New Phytol.* **226**, 1550–1566 (2020).
50. Berdugo, M. et al. Global ecosystem thresholds driven by aridity. *Science* **367**, 787–790 (2020).
51. Keenan, T. F., Luo, X., Zhang, Y. & Zhou, S. Ecosystem aridity and atmospheric CO₂. *Science* **368**, 251–252 (2020).
52. Yao, J. et al. Accelerated dryland expansion regulates future variability in dryland gross primary production. *Nat. Commun.* **11**, 1665 (2020).
53. Trenberth, K. E. et al. Global warming and changes in drought. *Nat. Clim. Change* **4**, 17–22 (2013).
54. Milly, P. C. D. & Dunne, K. A. Potential evapotranspiration and continental drying. *Nat. Clim. Change* **6**, 946–949 (2016).
55. Milly, P. & Dunne, K. A. A hydrologic drying bias in water-resource impact analyses of anthropogenic climate change. *J. Am. Water Resour. Assoc.* **53**, 822–838 (2017).
56. De Jeu, R. A. et al. Global soil moisture patterns observed by space borne microwave radiometers and scatterometers. *Surv. Geophys.* **29**, 399–420 (2008).
57. Berg, A. & Sheffield, J. Climate change and drought: the soil moisture perspective. *Curr. Clim. Change Rep.* **4**, 180–191 (2018).
58. Feng, H. & Zhang, M. Global land moisture trends: drier in dry and wetter in wet over land. *Sci. Rep.* **5**, 18018 (2015).
59. Berg, A., Sheffield, J. & Milly, P. C. D. Divergent surface and total soil moisture projections under global warming. *Geophys. Res. Lett.* **44**, 236–244 (2017).
60. Cook, B. I. et al. Twenty-first century drought projections in the CMIP6 forcing scenarios. *Earths Future* **8**, e2019EF001461 (2020).
61. Li, M., Wu, P., Ma, Z., Lv, M. & Yang, Q. Changes in soil moisture persistence in China over the past 40 years under a warming climate. *J. Clim.* **33**, 9531–9550 (2020).
62. Rodell, M. et al. Emerging trends in global freshwater availability. *Nature* **557**, 651–659 (2018).
63. Dai, A., Zhao, T. & Chen, J. Climate change and drought: a precipitation and evaporation perspective. *Curr. Clim. Change Rep.* **4**, 301–312 (2018).
Highlights the dominant role of CO₂ radiative forcing in shaping global land surface drying patterns for the twenty-first century.
64. Schlaepfer, D. R. et al. Climate change reduces extent of temperate drylands and intensifies drought in deep soils. *Nat. Commun.* **8**, 14196 (2017).
65. Li, L. et al. Global trends in water and sediment fluxes of the world's large rivers. *Sci. Bull.* **65**, 62–69 (2019).
66. Yang, H. et al. Regional patterns of future runoff changes from Earth system models constrained by observation. *Geophys. Res. Lett.* **44**, 5540–5549 (2017).
67. Wang, S. et al. Reduced sediment transport in the Yellow River due to anthropogenic changes. *Nat. Geosci.* **9**, 38–41 (2015).
68. Milly, P. C. D. & Dunne, K. A. Colorado River flow dwindles as warming-driven loss of reflective snow energizes evaporation. *Science* **367**, 1252–1255 (2020).
69. Trancoso, R., Larsen, J. R., McVicar, T. R., Phinn, S. R. & McAlpine, C. A. CO₂-vegetation feedbacks and other climate changes implicated in reducing base flow. *Geophys. Res. Lett.* **44**, 2310–2318 (2017).
70. Dai, A., Qian, T., Trenberth, K. E. & Milliman, J. D. Changes in continental freshwater discharge from 1948 to 2004. *J. Clim.* **22**, 2773–2792 (2009).
71. Hobeichi, S., Abramowitz, G., Evans, J. & Beck, H. E. Linear Optimal Runoff Aggregate (LORA): A global gridded synthesis runoff product. *Hydrol. Earth Syst. Sci.* **23**, 851–870 (2019).
72. Novick, K. A. et al. The increasing importance of atmospheric demand for ecosystem water and carbon fluxes. *Nat. Clim. Change* **6**, 1023–1027 (2016).
73. Chen, C. et al. China and India lead in greening of the world through land-use management. *Nat. Sustain.* **2**, 122–129 (2019).
74. Eyring, V. et al. Overview of the Coupled Model Intercomparison Project Phase 6 (CMIP6) experimental design and organization. *Geosci. Model Dev.* **9**, 1937–1958 (2016).
75. Eyring, V. et al. Taking climate model evaluation to the next level. *Nat. Clim. Change* **9**, 102–110 (2019).
76. Berg, A. et al. Land–atmosphere feedbacks amplify aridity increase over land under global warming. *Nat. Clim. Change* **6**, 869–874 (2016).
Reveals the important mechanism that declining soil moisture and altered vegetation physiology under climate change and rising CO₂ could make the near-surface air even warmer and drier.

77. Stephens, C. M., McVicar, T. R., Johnson, F. M. & Marshall, L. A. Revisiting pan evaporation trends in Australia a decade on. *Geophys. Res. Lett.* **45**, 11164–11172 (2018).
78. Byrne, M. P. & O’Gorman, P. A. The response of precipitation minus evapotranspiration to climate warming: why the “wet-get-wetter, dry-get-drier” scaling does not hold over land. *J. Clim.* **28**, 8078–8092 (2015).
79. Zhou, S. et al. Soil moisture–atmosphere feedbacks mitigate declining water availability in drylands. *Nat. Clim. Change* **11**, 38–44 (2020).
80. Lau, W. K. & Kim, K. M. Robust Hadley circulation changes and increasing global dryness due to CO₂ warming from CMIP5 model projections. *Proc. Natl Acad. Sci. USA* **112**, 3630–3635 (2015).
81. Lau, W. K. M. & Tao, W. Precipitation–radiation–circulation feedback processes associated with structural changes of the ITCZ in a warming climate during 1980–2014: an observational portrayal. *J. Clim.* **33**, 8737–8749 (2020).
82. Burls, N. J. & Fedorov, A. V. Wetter subtropics in a warmer world: contrasting past and future hydrological cycles. *Proc. Natl Acad. Sci. USA* **114**, 12888–12893 (2017).
83. Condon, L. E., Atchley, A. L. & Maxwell, R. M. Evapotranspiration depletes groundwater under warming over the contiguous United States. *Nat. Commun.* **11**, 873 (2020).
84. Jung, M. et al. Recent decline in the global land evapotranspiration trend due to limited moisture supply. *Nature* **467**, 951–954 (2010).
85. García, M. et al. Actual evapotranspiration in drylands derived from in-situ and satellite data: Assessing biophysical constraints. *Remote Sens. Environ.* **131**, 103–118 (2013).
86. Betts, R. A. et al. Projected increase in continental runoff due to plant responses to increasing carbon dioxide. *Nature* **448**, 1037–1041 (2007).
87. Swann, A. L., Hoffman, F. M., Koven, C. D. & Randerson, J. T. Plant responses to increasing CO₂ reduce estimates of climate impacts on drought severity. *Proc. Natl Acad. Sci. USA* **113**, 10019–10024 (2016).
88. Fowler, M. D., Kooperman, G. J., Randerson, J. T. & Pritchard, M. S. The effect of plant physiological responses to rising CO₂ on global streamflow. *Nat. Clim. Change* **9**, 873–879 (2019).
89. Lemordant, L., Gentine, P., Swann, A. S., Cook, B. I. & Scheff, J. Critical impact of vegetation physiology on the continental hydrologic cycle in response to increasing CO₂. *Proc. Natl Acad. Sci. USA* **115**, 4093–4098 (2018).
90. Haverd, V. et al. Higher than expected CO₂ fertilization inferred from leaf to global observations. *Glob. Change Biol.* **26**, 2390–2402 (2020).
91. Nie, M., Lu, M., Bell, J., Raut, S. & Pendall, E. Altered root traits due to elevated CO₂: a meta-analysis. *Glob. Ecol. Biogeogr.* **22**, 1095–1105 (2013).
92. Zhang, Y. et al. Multi-decadal trends in global terrestrial evapotranspiration and its components. *Sci. Rep.* **6**, 19124 (2016).
93. Sun, X., Wilcox, B. P. & Zou, C. B. Evapotranspiration partitioning in dryland ecosystems: A global meta-analysis of in situ studies. *J. Hydrol.* **576**, 123–136 (2019).
94. Lian, X. et al. Partitioning global land evapotranspiration using CMIP5 models constrained by observations. *Nat. Clim. Change* **8**, 640–646 (2018).
95. Yang, H., Huntingford, C., Wiltshire, A., Stith, S. & Mercado, L. Compensatory climate effects link trends in global runoff to rising atmospheric CO₂ concentration. *Environ. Res. Lett.* **14**, 124075 (2019).
96. Mankin, J. S. et al. Blue water trade-offs with vegetation in a CO₂-enriched climate. *Geophys. Res. Lett.* **45**, 3115–3125 (2018).
97. Stocker, B. D. et al. Quantifying soil moisture impacts on light use efficiency across biomes. *New Phytol.* **218**, 1430–1449 (2018).
98. Liu, L. et al. Soil moisture dominates dryness stress on ecosystem production globally. *Nat. Commun.* **11**, 4892 (2020).
99. Morgan, J. A. et al. C₄ grasses prosper as carbon dioxide eliminates desiccation in warmed semi-arid grassland. *Nature* **476**, 202–205 (2011).
100. Farrion, C. E., Rodriguez-Iturbide, I., Dybzinski, R., Levin, S. A. & Pacala, S. W. Decreased water limitation under elevated CO₂ amplifies potential for forest carbon sinks. *Proc. Natl Acad. Sci. USA* **112**, 7213–7218 (2015).
101. Lu, X., Wang, L. & McCabe, M. F. Elevated CO₂ as a driver of global dryland greening. *Sci. Rep.* **6**, 20716 (2016).
102. Ukkola, A. M., Keenan, T. F., Kelley, D. I. & Prentice, I. C. Vegetation plays an important role in mediating future water resources. *Environ. Res. Lett.* **11**, 094022 (2016).
103. Mankin, J. S., Smerdon, J. E., Cook, B. I., Williams, A. P. & Seager, R. The curious case of projected twenty-first-century drying but greening in the American West. *J. Clim.* **30**, 8689–8710 (2017).
104. Zarakas, C. M., Swann, A. L. S., Laguë, M. M., Armour, K. C. & Randerson, J. T. Plant physiology increases the magnitude and spread of the transient climate response to CO₂ in CMIP6 Earth system models. *J. Clim.* **33**, 8561–8578 (2020).
105. Mankin, J. S., Seager, R., Smerdon, J. E., Cook, B. I. & Williams, A. P. Mid-latitude freshwater availability reduced by projected vegetation responses to climate change. *Nat. Geosci.* **12**, 983–988 (2019).
106. Song, J. et al. Elevated CO₂ does not stimulate carbon sink in a semi-arid grassland. *Ecol. Lett.* **22**, 458–468 (2019).
107. Obermeier, W. A. et al. Reduced CO₂ fertilization effect in temperate C₃ grasslands under more extreme weather conditions. *Nat. Clim. Change* **7**, 137–141 (2016).
108. Craine, J. M. et al. Isotopic evidence for oligotrophication of terrestrial ecosystems. *Nat. Ecol. Evol.* **2**, 1735–1744 (2018).
109. Medlyn, B. E. et al. How do leaf and ecosystem measures of water-use efficiency compare? *New Phytol.* **216**, 758–770 (2017).
110. Keenan, T. F. et al. Increase in forest water-use efficiency as atmospheric carbon dioxide concentrations rise. *Nature* **499**, 324–327 (2013).
111. Peters, W. et al. Increased water-use efficiency and reduced CO₂ uptake by plants during droughts at a continental-scale. *Nat. Geosci.* **11**, 744–748 (2018).
112. Skinner, C. B., Poulsen, C. J. & Mankin, J. S. Amplification of heat extremes by plant CO₂ physiological forcing. *Nat. Commun.* **9**, 1094 (2018).
113. Lemordant, L. & Gentine, P. Vegetation response to rising CO₂ impacts extreme temperatures. *Geophys. Res. Lett.* **46**, 1385–1392 (2019).
114. Sellers, P. J. et al. Comparison of radiative and physiological effects of doubled atmospheric CO₂ on climate. *Science* **271**, 1402–1406 (1996).
115. Warren, J. M., Norby, R. J. & Wullschlegel, S. D. Elevated CO₂ enhances leaf senescence during extreme drought in a temperate forest. *Tree Physiol.* **31**, 117–130 (2011).
116. De Kauwe, M. G. et al. Examining the evidence for decoupling between photosynthesis and transpiration during heat extremes. *Biogeosciences* **16**, 903–916 (2019).
117. Huang, M. et al. Air temperature optima of vegetation productivity across global biomes. *Nat. Ecol. Evol.* **3**, 772–779 (2019).
118. Reich, P. B., Hobbie, S. E., Lee, T. D. & Pastore, M. A. Unexpected reversal of C₃ versus C₄ grass response to elevated CO₂ during a 20-year field experiment. *Science* **360**, 317–320 (2018).
119. Norby, R. J. et al. Model-data synthesis for the next generation of forest free-air CO₂ enrichment (FACE) experiments. *New Phytol.* **209**, 17–28 (2016).
120. Steffen, W. et al. The emergence and evolution of Earth System Science. *Nat. Rev. Earth Environ.* **1**, 54–63 (2020).
121. Hoekstra, A. Y. & Mekonnen, M. M. The water footprint of humanity. *Proc. Natl Acad. Sci. USA* **109**, 3232–3237 (2012).
122. Marvel, K. et al. Twentieth-century hydroclimate changes consistent with human influence. *Nature* **569**, 59–65 (2019).
123. Di Baldassarre, G. et al. Sociohydrology: scientific challenges in addressing the sustainable development goals. *Water Resour. Res.* **55**, 6327–6355 (2019).
124. van der Esch, S. et al. *Exploring Future Changes in Land Use and Land Condition and the Impacts on Food, Water, Climate Change and Biodiversity: Scenarios for the UNCCD Global Land Outlook* (PBL Netherlands Environmental Assessment Agency, 2017).
125. Gleick, P. H. Transitions to freshwater sustainability. *Proc. Natl Acad. Sci. USA* **115**, 8863–8871 (2018).
126. Wada, Y., de Graaf, I. E. M. & van Beek, L. P. H. High-resolution modeling of human and climate impacts on global water resources. *J. Adv. Model Earth Syst.* **8**, 735–763 (2016).
127. Wada, Y. et al. Modeling global water use for the 21st century: the Water Futures and Solutions (WfS) initiative and its approaches. *Geosci. Model Dev.* **9**, 175–222 (2016).
- Provides an ensemble model projection of significant increases in the twenty-first century’s water demand by major water-use sectors under envisaged population growth and socio-economic developments.**
128. Wada, Y., van Beek, L. P. H. & Bierkens, M. F. P. Nonsustainable groundwater sustaining irrigation: a global assessment. *Water Resour. Res.* **48**, W00L06 (2012).
129. Chen, Y. et al. Recent global cropland water consumption constrained by observations. *Water Resour. Res.* **55**, 3708–3738 (2019).
130. Allen, L. H. Jr., Kakani, V. G., Vu, J. C. & Boote, K. J. Elevated CO₂ increases water use efficiency by sustaining photosynthesis of water-limited maize and sorghum. *J. Plant Physiol.* **168**, 1909–1918 (2011).
131. Elliott, J. et al. Constraints and potentials of future irrigation water availability on agricultural production under climate change. *Proc. Natl Acad. Sci. USA* **111**, 3239–3244 (2014).
132. Urban, D. W., Sheffield, J. & Lobell, D. B. Historical effects of CO₂ and climate trends on global crop water demand. *Nat. Clim. Change* **7**, 901–905 (2017).
133. Gleeson, T., Wada, Y., Bierkens, M. F. & van Beek, L. P. Water balance of global aquifers revealed by groundwater footprint. *Nature* **488**, 197–200 (2012).
134. Bierkens, M. F. P. & Wada, Y. Non-renewable groundwater use and groundwater depletion: a review. *Environ. Res. Lett.* **14**, 063002 (2019).
135. Rodell, M., Velicogna, I. & Famiglietti, J. S. Satellite-based estimates of groundwater depletion in India. *Nature* **460**, 999–1002 (2009).
136. Feng, W. et al. Evaluation of groundwater depletion in North China using the Gravity Recovery and Climate Experiment (GRACE) data and ground-based measurements. *Water Resour. Res.* **49**, 2110–2118 (2013).
137. Eamus, D. & Friend, R. Groundwater-dependent ecosystems: the where, what and why of GDEs. *Aust. J. Bot.* **54**, 91–96 (2006).
138. Griebler, C. & Avramov, M. Groundwater ecosystem services: a review. *Freshw. Sci.* **34**, 355–367 (2015).
139. Devitt, T. J., Wright, A. M., Cannatella, D. C. & Hillis, D. M. Species delimitation in endangered groundwater salamanders: implications for aquifer management and biodiversity conservation. *Proc. Natl Acad. Sci. USA* **116**, 2624–2633 (2019).
140. Feng, X. et al. Revegetation in China’s Loess Plateau is approaching sustainable water resource limits. *Nat. Clim. Change* **6**, 1019–1022 (2016).
141. Hong, S. et al. Divergent responses of soil organic carbon to afforestation. *Nat. Sustain.* **3**, 694–700 (2020).
142. McVicar, T. R. et al. Developing a decision support tool for China’s re-vegetation program: Simulating regional impacts of afforestation on average annual streamflow in the Loess Plateau. *For. Ecol. Manag.* **251**, 65–81 (2007).
143. Zhao, M. et al. Ecological restoration impact on total terrestrial water storage. *Nat. Sustain.* **4**, 56–62 (2020).
144. Kwon, H.-Y. et al. *Economics of Land Degradation and Improvement – A Global Assessment for Sustainable Development* Ch. 8 (eds Nkonya E., Mirzabaev A. & von Braun J.) 197–214 (Springer, 2016).
145. Asner, G. P., Elmore, A. J., Olander, L. P., Martin, R. E. & Harris, A. T. Grazing systems, ecosystem responses, and global change. *Annu. Rev. Environ. Resour.* **29**, 261–299 (2004).
146. Dunne, T., Western, D. & Dietrich, W. E. Effects of cattle trampling on vegetation, infiltration, and erosion in a tropical rangeland. *J. Arid. Environ.* **75**, 58–69 (2011).
147. Griscom, B. W. et al. Natural climate solutions. *Proc. Natl Acad. Sci. USA* **114**, 11645–11650 (2017).
148. Lewis, S. L., Wheeler, C. E., Mitchard, E. T. & Koch, A. Restoring natural forests is the best way to remove atmospheric carbon. *Nature* **568**, 25–28 (2019).
149. Reisman-Berman, O., Keasar, T. & Tel-Zur, N. Native and non-native species for dryland afforestation: bridging ecosystem integrity and livelihood support. *Ann. For. Sci.* **76**, 114 (2019).
150. Zhang, J. et al. Carrying capacity for vegetation across northern China drylands. *Sci. Total Environ.* **710**, 136391 (2020).
151. Liu, Y., Kumar, M., Katul, G. G. & Porporato, A. Reduced resilience as an early warning signal of forest mortality. *Nat. Clim. Change* **9**, 880–885 (2019).
152. Fita, A., Rodriguez-Burruezo, A., Boscaiu, M., Prohens, J. & Vicente, O. Breeding and domesticating crops adapted to drought and salinity: a new paradigm for increasing food production. *Front. Plant Sci.* **6**, 978 (2015).

153. Graham, N. T. et al. Water sector assumptions for the Shared Socioeconomic Pathways in an integrated modeling framework. *Water Resour. Res.* **54**, 6423–6440 (2018).
154. Muhs, D. R. The geologic records of dust in the Quaternary. *Aeolian Res.* **9**, 3–48 (2013).
155. Scheff, J., Seager, R., Liu, H. & Coats, S. Are glacials dry? Consequences for paleoclimatology and for greenhouse warming. *J. Clim.* **30**, 6593–6609 (2017).
156. Lambert, F. et al. Dust-climate couplings over the past 800,000 years from the EPICA Dome C ice core. *Nature* **452**, 616–619 (2008).
157. Salzmann, U. et al. Climate and environment of a Pliocene warm world. *Palaeogeogr. Palaeoclimatol. Palaeoecol.* **309**, 1–8 (2011).
158. Fu, Q., Lin, L., Huang, J., Feng, S. & Gettelman, A. Changes in terrestrial aridity for the period 850–2080 from the Community Earth System Model. *J. Geophys. Res. Atmos.* **121**, 2857–2873 (2016).
159. Prudhomme, C. et al. Hydrological droughts in the 21st century, hotspots and uncertainties in a global multimodel ensemble experiment. *Proc. Natl Acad. Sci. USA* **111**, 3262–3267 (2014).
160. Cook, B. I., Ault, T. R. & Smerdon, J. E. Unprecedented 21st century drought risk in the American Southwest and Central Plains. *Sci. Adv.* **1**, e1400082 (2015).
161. Ault, T. R. On the essentials of drought in a changing climate. *Science* **368**, 256–260 (2020).
162. Reichstein, M. et al. Climate extremes and the carbon cycle. *Nature* **500**, 287–295 (2013).
163. Anderegg, W. R. L., Kane, J. M. & Anderegg, L. D. L. Consequences of widespread tree mortality triggered by drought and temperature stress. *Nat. Clim. Change* **3**, 30–36 (2012).
164. Williams, A. P. et al. Forest responses to increasing aridity and warmth in the southwestern United States. *Proc. Natl Acad. Sci. USA* **107**, 21289–21294 (2010).
165. Pellegrini, A. F. A. et al. Fire frequency drives decadal changes in soil carbon and nitrogen and ecosystem productivity. *Nature* **553**, 194–198 (2018).
166. Bowman, D. M. J. S. et al. Vegetation fires in the Anthropocene. *Nat. Rev. Earth Environ.* **1**, 500–515 (2020).
167. Andela, N. et al. A human-driven decline in global burned area. *Science* **356**, 1356–1362 (2017).
168. Pechony, O. & Shindell, D. T. Driving forces of global wildfires over the past millennium and the forthcoming century. *Proc. Natl Acad. Sci. USA* **107**, 19167–19170 (2010).
169. Hoover, D. L., Knapp, A. K. & Smith, M. D. Resistance and resilience of a grassland ecosystem to climate extremes. *Ecology* **95**, 2646–2656 (2014).
170. Greve, P. et al. Global assessment of water challenges under uncertainty in water scarcity projections. *Nat. Sustain.* **1**, 486–494 (2018).
171. Scanlon, B. R. et al. Global models underestimate large decadal declining and rising water storage trends relative to GRACE satellite data. *Proc. Natl Acad. Sci. USA* **115**, E1080–E1089 (2018).
172. Abatzoglou, J. T., Dobrowski, S. Z., Parks, S. A. & Hegewisch, K. C. TerraClimate, a high-resolution global dataset of monthly climate and climatic water balance from 1958–2015. *Sci. Data* **5**, 170191 (2018).
173. Roderick, M. L., Sun, F., Lim, W. H. & Farquhar, G. D. A general framework for understanding the response of the water cycle to global warming over land and ocean. *Hydrol. Earth Syst. Sci.* **18**, 1575–1589 (2014).
174. Gudmundsson, L., Greve, P. & Seneviratne, S. I. The sensitivity of water availability to changes in the aridity index and other factors—A probabilistic analysis in the Budyko space. *Geophys. Res. Lett.* **43**, 6985–6994 (2016).
175. American Meteorological Society. *Glossary of Meteorology* <http://glossary.ametsoc.org/wiki/Aridity> (2000).
176. Allen, R. G., Pereira, L. S., Raes, D. & Smith, M. *Crop Evapotranspiration — Guidelines for Computing Crop Water Requirements — FAO Irrigation and Drainage Paper 56* (Food and Agriculture Organization of the United Nations, 1998).
177. Dai, A. Drought under global warming: a review. *Wiley Interdiscip. Rev. Clim. Change* **2**, 45–65 (2011).
178. Dai, A. In *Terrestrial Water Cycle and Climate Change: Natural and Human-Induced Impacts* 1st edn, Ch. 2 (eds Tang, Q. & Oki, T.) 17–37 (Wiley, 2016).
179. Sitoh, S. et al. Trends and drivers of regional sources and sinks of carbon dioxide over the past two decades. *Biogeosci. Discuss.* **10**, 20113–20177 (2013).
180. Donohue, R. J., Roderick, M. L., McVicar, T. R. & Yang, Y. A simple hypothesis of how leaf and canopy-level transpiration and assimilation respond to elevated CO₂ reveals distinct response patterns between disturbed and undisturbed vegetation. *J. Geophys. Res. Biogeosci.* **122**, 168–184 (2017).
181. Barton, C. V. M. et al. Effects of elevated atmospheric [CO₂] on instantaneous transpiration efficiency at leaf and canopy scales in *Eucalyptus saligna*. *Glob. Change Biol.* **18**, 585–595 (2012).
182. Savvides, A. M. & Fotopoulos, V. Two inexpensive and non-destructive techniques to correct for smaller-than-gasket leaf area in gas exchange measurements. *Front. Plant Sci.* **9**, 548 (2018).

Acknowledgements

This study was supported by the National Natural Science Foundation of China (41991230, 41988101), the Second Tibetan Plateau Scientific Expedition and Research (STEP) program (grant no. 2019QZKK0405) and the Xplorer Prize.

Author contributions

S.P. formulated the Review and identified the themes to be covered. X.L. performed the analyses and drafted the figures. X.L., S.P. and A.C. wrote the first draft of the manuscript. C.H., B.F., L.Z.X.L., J.H., J.S., A.M.B., T.F.K., T.R.M., Y.W., X.W., T.W., Y.Y. and M.L.R. reviewed and edited the manuscript before submission. All authors made substantial contributions to the discussion of content.

Competing interests

The authors declare no competing interests.

Peer review information

Nature Reviews Earth & Environment thanks Aristeidis Koutroulis, Sujong Jeong and the other, anonymous, reviewer(s) for their contribution to the peer review of this work.

Publisher's note

Springer Nature remains neutral with regard to jurisdictional claims in published maps and institutional affiliations.

Supplementary information

The online version contains supplementary material available at <https://doi.org/10.1038/s43017-021-00144-0>.

© Springer Nature Limited 2021

QUERY FORM

Nature Reviews Earth & Environment	
Manuscript ID	144
Author	Xu Lian

AUTHOR:

The following queries have arisen during the editing of your manuscript. Please answer by making the requisite corrections directly in the e-proofing tool rather than marking them up on the PDF. This will ensure that your corrections are incorporated accurately and that your paper is published as quickly as possible.

Query No.	Nature of Query
Q1:	Please check your article carefully, coordinate with any co-authors and enter all final edits clearly in the eproof, remembering to save frequently. Once corrections are submitted, we cannot routinely make further changes to the article.
Q2:	Note that the eproof should be amended in only one browser window at any one time; otherwise changes will be overwritten.
Q3:	Author surnames have been highlighted. Please check these carefully and adjust if the first name or surname is marked up incorrectly. Note that changes here will affect indexing of your article in public repositories such as PubMed. Also, carefully check the spelling and numbering of all author names and affiliations, and the corresponding email address(es).
Q4:	You cannot alter accepted Supplementary Information files except for critical changes to scientific content. If you do resupply any files, please also provide a brief (but complete) list of changes. If these are not considered scientific changes, any altered Supplementary files will not be used, only the originally accepted version will be published.